Plant Communications
Research article

CellPress
Partner Journal

Phenomics-assisted genetic dissection and molecular design of drought resistance in rice

Qiaojun Lou[1,3,5,7], Yunyu Chen[2,7], Xin Wang[1,2,7], Yulu Zhang[2], Tingting Gao[2], Jiawei Shi[2], Ming Yan[1,5], Fangjun Feng[1,5], Kai Xu[1,5], Feng Lin[4], Shangyuan Xie[2], Xiaoyan Xi[2], Weikun Li[2], Yuanyuan Nie[6], Huan Gao[1,5], Hui Xia[1,5], Lei Wang[1,5], Tiemei Li[1,5], Shoujun Chen[1,5], Ying Zhu[3], Jianwei Zhang[2], Hanwei Mei[1,5], Liang Chen[1,5,*], Wanneng Yang[2,*] and Lijun Luo[1,5,*]

[1]Shanghai Agrobiological Gene Center, Shanghai 201106, China

[2]National Key Laboratory of Crop Genetic Improvement, National Center of Plant Gene Research, Hubei Hongshan Laboratory, Huazhong Agricultural University, Wuhan 430070, China

[3]State Key Laboratory for Managing Biotic and Chemical Threats to the Quality and Safety of Agro-Products, Institute of Virology and Biotechnology, Zhejiang Academy of Agricultural Sciences, Hangzhou 310021, China

[4]Zhejiang University, Hangzhou 310058, China

[5]Key Laboratory of Grain Crop Genetic Resources Evaluation and Utilization, Ministry of Agriculture and Rural Affairs, Shanghai 201106, China

[6]Jiangxi Research and Development Center of Super Rice, Nanchang Branch of Chinese National Center for Rice Improvement, Nanchang 330200, China

[7]These authors contributed equally to this article.

***Correspondence: Liang Chen (cl@sagc.org.cn), Wanneng Yang (ywn@mail.hzau.edu.cn), Lijun Luo (lijun@sagc.org.cn)**

https://doi.org/10.1016/j.xplc.2024.101218

ABSTRACT

Dissecting the mechanism of drought resistance (DR) and designing drought-resistant rice varieties are promising strategies to address the challenge of climate change. Here, we selected a typical drought-avoidant (DA) variety, IRAT109, and a drought-tolerant (DT) variety, Hanhui15, as parents to develop a stable recombinant inbred line (RIL) population (F_8, 1262 lines). The *de novo* assembled genomes of both parents were released. By resequencing of the RIL population, a set of 1 189 216 reliable SNPs were obtained and used to construct a dense genetic map. Using above- and belowground phenomic platforms and multimodal cameras, we captured 139 040 image-based traits (i-traits) of whole-plant phenotypes in response to drought stress throughout the entire rice growth period and identified 32 586 drought-responsive quantitative trait loci (QTLs), including 2097 unique QTLs. QTLs associated with panicle i-traits occurred more than 600 times on the middle of chromosome 8, and QTLs associated with leaf i-traits occurred more than 800 times on the 5′ end of chromosome 3, indicating the potential effects of these QTLs on plant phenotypes. We selected three candidate genes (*OsMADS50*, *OsGhd8*, *OsSAUR11*) related to leaf, panicle, and root traits, respectively, and verified their functions in DR. *OsMADS50* was found to negatively regulate DR by modulating leaf dehydration, grain size, and downward root growth. A total of 18 and 21 composite QTLs significantly related to grain weight and plant biomass were also screened from 597 lines in the RIL population under drought conditions in field experiments, and the composite QTL regions showed substantial overlap (76.9%) with known DR gene regions. Based on three candidate DR genes, we proposed a haplotype design suitable for different environments and breeding objectives. This study provides a valuable reference for multimodal and time-series phenomic analyses, deciphers the genetic mechanisms of DA and DT rice varieties, and offers a molecular navigation map for breeding of DR varieties.

Key words: drought resistance, *de novo* drought-resistant rice genomes, high-throughput phenomics, whole-plant image traits, multimodal camera, quantitative trait loci, QTLs, molecular design

Lou Q., Chen Y., Wang X., Zhang Y., Gao T., Shi J., Yan M., Feng F., Xu K., Lin F., Xie S., Xi X., Weikun Li, Nie Y., Gao H., Xia H., Wang L., Li T., Chen S., Zhu Y., Zhang J., Mei H., Chen L., Yang W., and Luo L. (2025). Phenomics-assisted genetic dissection and molecular design of drought resistance in rice. Plant Comm. **6**, 101218.

Published by the Plant Communications Shanghai Editorial Office in association with Cell Press, an imprint of Elsevier Inc., on behalf of CSPB and CEMPS, CAS.

Please cite this article in press as: Lou et al., Phenomics-assisted genetic dissection and molecular design of drought resistance in rice, Plant Communications (2024), https://doi.org/10.1016/j.xplc.2024.101218

INTRODUCTION

With the increasing extreme weather in recent years, world food security has been severely threatened (Pollmann et al., 2019). Rice is the main grain crop supporting more than half of the global population, but rice production is vulnerable to climate change (Sreenivasulu et al., 2015). Among all abiotic stresses, drought stress (DS) causes serious yield reductions (Yang et al., 2022b). Moreover, planting rice with good drought resistance (DR) can save irrigation water and reduce methane (CH_4) release in non-flooding fields (Xia et al., 2022). Therefore, dissecting the drought-resistance mechanism of rice and cultivating drought-resistant rice varieties represent a promising strategy to address the challenge of climate change.

DR is a complex trait that involves various physiological, biochemical, and genetic responses and can be influenced by a large number of micro-effect loci (Blum, 2010; Fukao and Xiong, 2013). Under DS, rice plants undergo a series of phenotypic changes such as rolling and withering of leaves, morphological changes in roots, delayed flowering, and reduced biomass and yield (Kim et al., 2020; Bhandari et al., 2023). A large number of drought-related loci have been mapped by quantitative trait locus (QTL) analysis and candidate gene cloning in rice (Champoux et al., 1995; Price et al., 1997; Yue et al., 2006; Khowaja and Price, 2008; Guo et al., 2018). Cloned DR genes can affect multiple biological processes such as cell-wall composition, reactive oxygen species scavenging, stomatal closure, hormonal regulation, and deep rooting (Seo et al., 2011; Uga et al., 2013, 2015; You et al., 2013; Li et al., 2017; Xiong et al., 2018; Yu et al., 2018). However, there have been few comprehensive reports on whole-plant responses to drought throughout the entire rice growth cycle.

There are four inherent mechanisms of DR: drought avoidance (DA), drought tolerance (DT), drought recovery, and drought escape (Luo and Zhang, 2001). These mechanisms jointly determine plant performance under DS. In most cases, DA and DT are the main mechanisms that affect plant DR. DA contributes to the maintenance of high water potential in plants through water absorption by strong roots and reductions in canopy water loss. DT assists plants in maintaining normal physiological functions in the case of low water potential mainly through osmotic adjustment (Luo, 2010). Therefore, the belowground root system performs major functions in DA, whereas the aboveground leaf and panicle are the main organs involved in the response to DS through DT. Genetic research based on refined genome assemblies of typical DA and DT rice varieties and linkage mapping of their recombinant inbred line (RIL) populations can provide valuable genomic resources and a new perspective for investigating rice drought adaptability and breeding drought-resistant rice varieties.

A lack of phenotypic data has become the key bottleneck to the genetic dissection of important agronomic traits in crops (Araus et al., 2018; Song et al., 2021b). With the rapid development of imaging technologies and big data, phenomics is playing a more and more important role in crop research and breeding (Chen et al., 2014; Yang et al., 2020). Various automatic imaging equipment enables the collection of non-destructive, accurate, large-scale, and high-dimensional phenotypic data throughout the whole plant growth period (Houle et al., 2010; Tang et al., 2023; Yang et al., 2023). Considering the high complexity of plant responses to DS, a high-throughput phenotyping system with multimodal cameras seems to be the best choice for the simultaneous and non-destructive acquisition of multiple phenotypic features such as color, shape, texture, canopy temperature, flowering time, and yield. High-throughput phenotyping has proven to be an effective tool for investigating the genetic basis of DR at the population level across several plant species (Guo et al., 2018; Briglia et al., 2020; Li et al., 2020; Wu et al., 2021). However, little research has been performed to capture phenotypic changes in both aboveground and belowground plant parts in response to DS throughout the entire rice growth period by combining multiple imaging methods.

Molecular design represents a new trend in future breeding (Xu et al., 2012; Oladosu et al., 2019). Exploring the relationship between genes and the environment and the effects of genes on agronomic traits are very important for the design of drought-resistant varieties. For example, plants have evolved different mechanisms to resist DS in different environments. When crops are grown in an upland field without a hard plow pan, roots play an important role in resisting DS, because plant roots can absorb water from the deep soil. However, in lowland fields with a hard plow pan, the aboveground parts of crops may become more important than the belowground roots. Therefore, it is essential to obtain information related to different environments, different growth stages, and different organs to support the molecular design of drought-resistant varieties.

In our previous study, we developed a high-throughput phenomics platform (HTPP) to quantify DR-related phenotypic traits (Gao et al., 2022a, 2022b). On this HTPP, we can implement gradient drought treatments with plants from the same plot to ensure identical growth conditions (except for soil moisture). Moreover, the HTPP equipped with multimodal cameras can examine as many as 50 000 rice plants in a population simultaneously. In the present study, we comprehensively investigated aboveground and belowground traits related to DR and identified QTLs based on these traits. First, we selected two varieties with good DA and DT, respectively (Figure 1A), assembled their genomes *de novo*, and established a stable RIL population containing 1262 lines. All the RILs were resequenced to construct a high-density genetic map (Figure 1B). Second, we phenotyped 217 lines in the field and in root boxes under drought treatment at consecutive growth stages and screened out more than 50 000 highly heritable and drought-sensitive image traits (i-traits). Five hundred ninety-seven unused lines (out of 1262 lines) were manually phenotyped under drought in a natural field in Hainan province, China (Figure 1C). Third, more than 2000 unique DR QTLs were identified from i-traits using the transcriptomic data, three drought-related candidate genes were identified, and their functions in DR were determined (Figure 1D). Finally, we developed machine-learning-based models to predict the DR index. Through a chi-squared test, a number of QTLs identified by i-traits were also found to be correlated with rice yield under DS (Figure 1E). The superior alleles of these candidate genes were proposed for use in the molecular design of rice DR varieties. Assisted by phenomics, this study reports the largest number of rice DR QTLs identified to

Please cite this article in press as: Lou et al., Phenomics-assisted genetic dissection and molecular design of drought resistance in rice, Plant Communications (2024), https://doi.org/10.1016/j.xplc.2024.101218

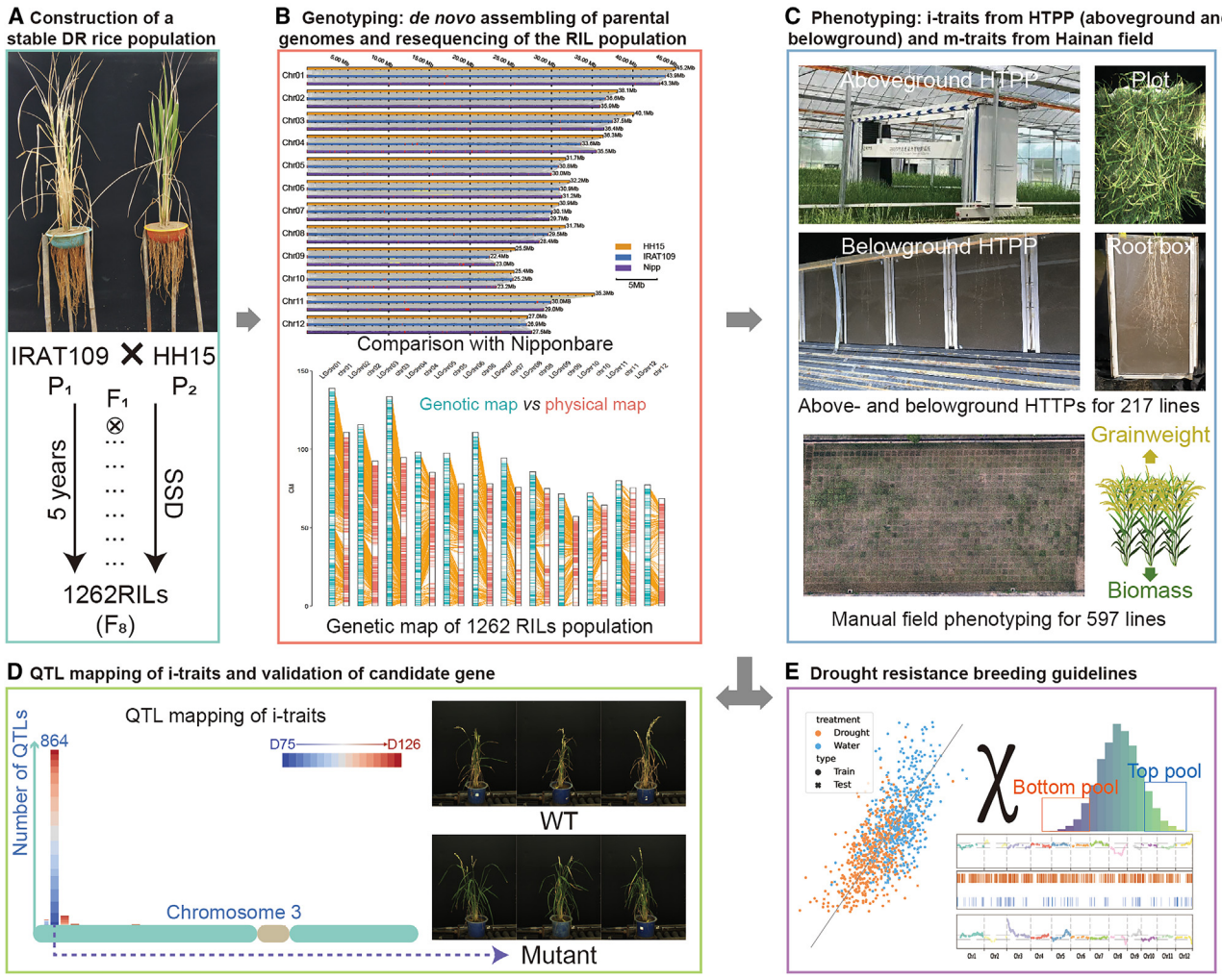

Figure 1. The main framework of this study.

(A) Construction of a stable recombinant inbred line (RIL) rice population using IRAT109 (P_1, a drought avoidant variety) and HH15 (P_2, a drought tolerant variety) as parents through the single-seed descent (SSD) method.

(B) Genotyping of the RIL population, including *de novo* assembly of the parental genomes and resequencing of the RIL population to construct a high-density genetic map. Upper graph: multicollinearity among the genomes of IRAT109 (orange), HH15 (blue), and Nipponbare (purple); gray and yellow lines represent collinearity and large inversions (>10 kb), respectively, and red blocks indicate genomic gaps. Lower graph: the high-density genetic map (green) is displayed alongside its collinearity with the physical map (red) of the variety IRAT109.

(C) Phenotyping 217 lines of the RIL population with above- and belowground high-throughput phenomics platforms (HTPPs) in Shanghai and Wuhan to capture whole-plant i-traits and by manual evaluation of drought resistance for the unused 597 lines under natural field conditions in Hainan province.

(D) Using genetic and phenotypic data from **(B)** and **(C)**, QTL mapping was performed to identify drought-resistance QTLs, and several candidate genes were selected for further functional validation. As an example, QTLs of RGB-derived leaf i-traits during the continuous drought treatment were mapped to chromosome 3 and validated with mutant materials.

(E) Breeding guidelines for drought resistance, including a predictive model of drought resistance based on image traits and the supply of some elite haplotypes.

date and provides useful genetic resources for breeding design aimed at improvement of rice DR.

RESULTS

Construction of a stable population with diverse DR capacities

Over the last two decades, we have collected a large number of drought-resistant rice germplasm resources from around the world (Lou et al., 2015; Wu et al., 2015). Through multiyear multisite phenotypic screening, IRAT109 and Hanhui15 (HH15) were found to be a typical DA variety and DT variety, respectively. IRAT109 (*japonica*, represented by P_1, which originated in Africa) possesses a deep root system, but it exhibits relatively poor DT when its root system is limited in a shallow soil layer or in pots. HH15 (*indica*, represented by P_2) is a water-saving and drought-tolerant rice (WDR) restorer line developed by Shanghai Agrobiological Gene Center (SAGC) that exhibits a desirable DT despite its shallow root system (Figure 1A and Supplemental Figure 1). These two representative lines with their distinct DA and DT traits were selected as parents to develop a stable

Please cite this article in press as: Lou et al., Phenomics-assisted genetic dissection and molecular design of drought resistance in rice, Plant Communications (2024), https://doi.org/10.1016/j.xplc.2024.101218

population of RILs using the single-seed descent (SSD) method. A total of 1262 stable RILs were developed through eight generations of self-crossing within five years.

Genotyping of the parents and population

Using second- and third-generation sequencing techniques, the genomes of both parents were assembled *de novo* and publicly released. The assembled HH15 genome reached a high-quality genome level with a BUSCO value of 98.7% and an LAI value of 23.46, and the IRAT109 genome also reached a high-quality genome level with a BUSCO value of 98.7% and an LAI value of 21.92. Compared with the Nipponbare genome (a *japonica* variety, the first and most widely used rice reference genome), our *indica* rice HH15 genome exhibited a greater total length (399 426 935 bp with only 10 gaps) (Figure 1B and Supplemental Table 1), whereas the *japonica* rice IRAT109 genome had a shorter total length (377 412 274 bp) with 77 gaps. Relative to the Nipponbare genome, genomes of both these drought-resistant rice varieties displayed several long inversions on chromosomes 6, 7, 8, and 9, such as the notable 5-Mb inversion in the middle of chromosome 6 in the IRAT109 genome. Through genome alignment of HH15 and IRAT109, we identified 2 268 907 SNPs and 421 111 InDels, with approximately 40% (915 368) of the SNPs located in gene regions (Supplemental Table 2). On the basis of transcriptome and proteome data, 61 947 genes were annotated in the HH15 genome and 55 498 genes in the IRAT109 genome. About 350.0 Mb (92.7%) of the IRAT109 genome sequences were highly collinear with 369.5 Mb (92.5%) of the HH15 genome sequences, involving 53 040 (95.6%) genes in the IRAT109 genome and 58 794 (94.9%) genes in the HH15 genome. Through comparison with the genomes of 17 other non-DA rice varieties, we identified 9209 genes as specific to the IRAT109 genome, and through comparison with the genomes of 17 other non-DT rice varieties, we identified 14 584 genes as specific to the HH15 genome (Supplemental Tables 3 and 4). These genes may therefore be specifically associated with DA or DT.

Through whole-genome resequencing of the RIL population (1262 lines), we obtained an average of 2.3 Gb of sequence data per line, with an average genome coverage of 91.43%. We identified 1 189 216 reliable SNPs, from which 11 785 bin markers were developed and used to construct a genetic linkage map with a total length of 1151.7 cM (Figure 1B). In the genetic linkage map, the average chromosome length was 95.98 cM; chromosome 9 was shortest (69.57 cM), and chromosome 1 was longest (136.79 cM). Because bin markers were evenly distributed with a short average genetic distance of 0.11 cM between adjacent markers, this genetic linkage map could be used for subsequent genetic mapping (Supplemental Table 5).

Population phenotyping

We collected aboveground and belowground phenotypic data in a continuous time series under DS and well-watered (WW) treatments (Figure 1C). For aboveground phenotype experiments, the HTPP was used to capture image-based traits (i-traits) using hyperspectral (HSI), infrared (IR), and visible-light (red, green, and blue light [RGB]) cameras at 17 time points from day 75 post sowing into the field (D75) to D126 in Jinshan, Shanghai. For belowground phenotype experiments, root i-traits were captured using a visible-light camera at nine time points from D21 to D45 post sowing into root boxes in Wuhan, Hubei. As drought became increasingly severe, differences were observed in the HSI, IR, and RGB images between DS and WW samples (Figure 2A). The WW samples had greater plant heights, earlier flowering, greener canopies, and shallower root distributions than the DS samples.

We developed an efficient pipeline for processing of image data in this study (Figure 2B and Supplemental Video 1). After image processing, 910 HSI-derived, 27 IR-derived, and 70 RGB-derived aboveground traits and 29 RGB-derived belowground (root) traits were obtained at one time point, and 17 380 aboveground and belowground i-traits were obtained across all sample collection time points (Supplemental Tables 6–8). The total number of DR-related raw i-traits was calculated as 17 380 × 2 (DS and DS/WW) × 4 (three replicates and their averages), which was 139 040. In addition, data for 10 yield-related traits were manually collected (Supplemental Table 9). All data were uploaded to a public website (http://plantphenomics.hzau.edu.cn/en/information).

As shown in Figure 3A, there were significant differences in the distributions of the 10 manually measured traits between the WW and DS treatments ($p < 0.05$). We selected four representative i-traits from a total of 1036 i-traits as phenotype traits in responses to DS: three aboveground i-traits and one belowground i-trait. "Water band index" (WBI) is an i-trait obtained by the HSI camera that shows high sensitivity to variations in canopy moisture status and is calculated according to the formula WBI = r_{900}/r_{970} (Peñuelas et al., 1997) (Figure 3B). Canopy temperature is a common indicator of DS (Yoshimoto et al., 2005). "Mean temperature" refers to the mean temperature of all the canopy pixels in an IR image (Figure 3C). The RGB-derived i-trait "TPA_panicle" denotes the projected area of panicles and represents panicle biomass (Figure 3D). The soil water potential was recorded in WW and DS plots using wireless soil water potential probes throughout the entire DS process (Figure 3E). During the early stage of drought (D75–D90), there were no significant differences in water potential between the WW and DS treatments and, accordingly, no significant differences in i-traits. As differences in water potential increased from D96 onward, differences in WBI ($p_{D75\ =\ 0.96,\ p_{D96\ =\ 1.63e-6)}}$, MeanTemperature ($p_{D75\ =\ 0.99,\ p_{D96\ =\ 3.60e-6)}}$, and TPA_panicle ($p_{D75\ =\ 0.25,\ p_{D96\ =\ 3.21e-3)}}$ between WW and DS treatments became increasingly significant. The trend in WBI during the late stage of drought (D96–D126) was consistent with the pattern of soil water potential. The difference in TPA_panicle between DS and WW remained stable after D111, perhaps because rice plants had completed heading by this time and panicle architecture therefore showed few changes. Although MeanTemperature was influenced by ambient temperature, the differences between WW and DS were stable, with consistently higher canopy temperatures in the DS plot than in the WW plot (Figure 3F). Root depth was a belowground i-trait, and the DS plants always had a deeper rooting depth than the WW plants as DS progressed ($p_{D21\ =\ 1.92e-6)}$. Taken together, our data demonstrate that the selected i-traits were sensitive to DS and could thus serve as indicators reflecting drought-induced variations. As shown in Figure 3G, most of the m-traits (manually measured traits; 8/10) had high heritability ($H > 0.5$), and the panicle-related traits showed clear correlations with TPA_panicle

Please cite this article in press as: Lou et al., Phenomics-assisted genetic dissection and molecular design of drought resistance in rice, Plant Communications (2024), https://doi.org/10.1016/j.xplc.2024.101218

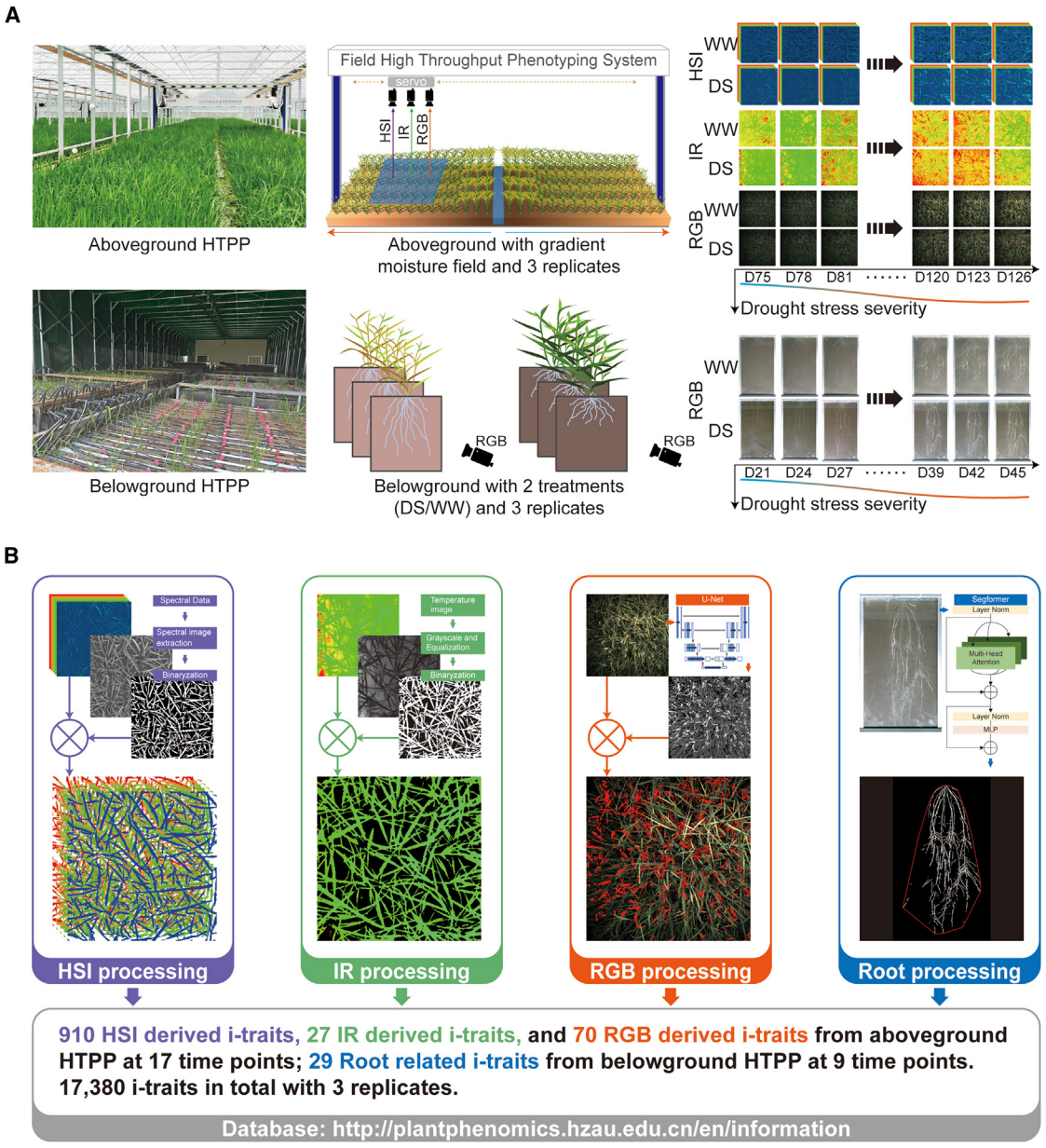

Figure 2. Pipeline for acquisition of i-traits (image traits).

(A) Phenomics platform and image capture. The automated phenotyping experiment consisted of two sections: aboveground (top half) and belowground (bottom half). The left panel shows the actual scenario of the phenomics experiment; the middle panel presents a schematic of the experimental design; and the right panel displays four series of images captured by hyperspectral (HSI), infrared (IR), and visible-light (red, green, and blue light [RGB]) cameras and belowground RGB cameras.

(B) Image processing and trait acquisition. The four schematic diagrams indicate the workflow for processing images from aboveground HSI, IR, and RGB and belowground RGB (root) images to obtain i-traits. All raw data are available at http://plantphenomics.hzau.edu.cn/en/information.

(R_{FGN} = 0.38, $R_{GrainWeight}$ = 0.41). The HSI-derived aboveground i-traits also tended to demonstrate high heritability ($H > 0.5$) (Figure 3H), whereas the IR-derived i-traits generally exhibited low heritability ($H < 0.3$), perhaps owing to the influence of environmental factors on canopy temperature (Figure 3I). Clustering analysis showed that the heritability of aboveground RGB-derived i-traits classified them into two distinct groups, panicle traits and leaf traits (Figure 3J). In general, panicle traits displayed lower heritability ($H < 0.3$) than leaf traits in the early drought stage (D75–D96) but higher heritability at the late drought stage (D99–D126) ($H > 0.5$). In addition, the belowground i-traits generally exhibited lower heritability than the aboveground i-traits ($H < 0.3$, Figure 3K). The heritability of belowground i-traits related to root length, mass, and density was higher than that of other belowground i-traits such as angle ($H > 0.3$).

In addition to automatic phenomics identification, we also evaluated DR manually in the field in Hainan province under natural DS (Figure 1C). This experiment included 597 lines from the RIL

Please cite this article in press as: Lou et al., Phenomics-assisted genetic dissection and molecular design of drought resistance in rice, Plant Communications (2024), https://doi.org/10.1016/j.xplc.2024.101218

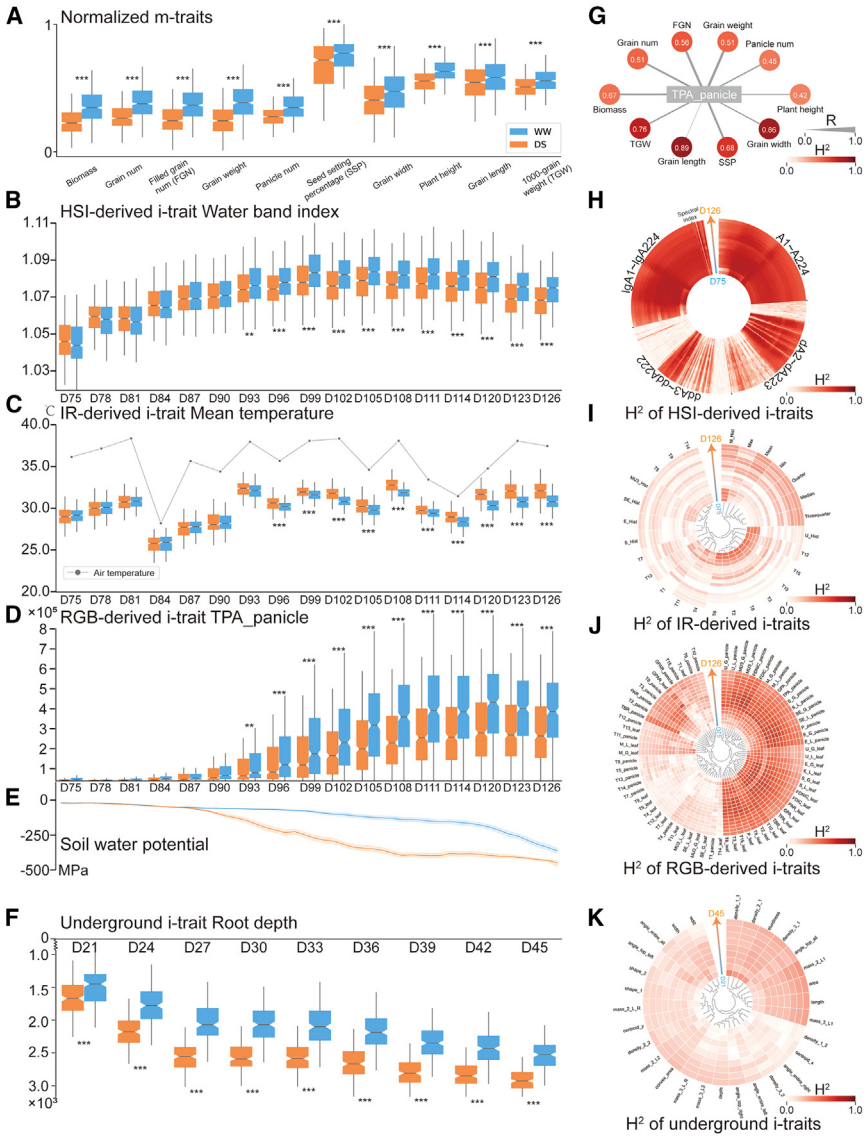

Figure 3. General demonstration and analysis of i-traits in response to drought.

(A) Manual trait distribution between WW and DS treatments.

(B–F) Temporal changes in aboveground i-traits derived from HSI **(B)**, IR **(C)**, and RGB **(D)** cameras, soil water potential **(E)**, and root depth **(F)** between WW and DS treatments. The gray line in **(C)** represents the ambient temperature.

(G) Broad heritability of the manual traits and their correlations with the i-trait TPA_panicle (TPA, total projected area).**(H–K)** Broad-sense heritability of aboveground HSI-derived **(H)**, IR-derived **(I)**, and RGB-derived **(J)** i-traits, as well as belowground i-traits **(K)**, at different time points. $^{**}p < 0.01$, $^{***}p < 0.001$ (*t*-test, $N = 651$).

population (out of 1262 lines; unused in the HTPP experiments) with three replicates (6 × 6 plants per plot). The mean aboveground dry weight per plant of the 597 lines was 104.67 g with a standard deviation of 18.02 g, and the average total grain weight per plant of the 597 lines was 11.49 g with a standard deviation of 6.89 g. These two traits were used for screening of reliable DR-related QTLs.

QTL mapping and candidate gene validation

After data preprocessing, 52 984 DR-related i-traits from various imaging sources and time points were selected for use in QTL mapping, including 41 912 (total 123 760) HSI-derived i-traits, 2268 (total 3672) IR-derived i-traits, 7732 (total 9520) RGB-derived i-traits, and 1072 (total 2088) root-related i-traits. From the 52 984 i-traits, we selected 18 976 i-traits for which at least one QTL had a likelihood of odds (LOD) score >2.5, and 32 586 significant QTLs were mapped from these 18 976 i-traits (Figure 4A and Supplemental Table 10). As shown in Figure 4A, root trait-related QTLs were mostly located on chromosomes 2, 3, 9, and 12. Among these, chromosome 2 had the largest number of QTLs (up to 128), accounting for about 26.9% of all root-related QTLs. Most QTLs appeared in the late growth stage. Regions where aboveground and belowground QTLs co-localized were densely distributed on chromosomes 2, 3, 9, and 12, suggesting that these co-localized QTLs might be genetic loci that influence both aboveground and belowground phenotypes. This possibility will require further investigation in future DR studies and breeding efforts. HSI-derived QTLs were predominantly distributed on chromosomes 3, 5, 8, 9, and 11, with a 5-Mb region of chromosome 8 exhibiting the densest QTL distribution. Different QTL distribution patterns were observed at different DS stages. For example, QTLs were detectable on chromosome 3 throughout the entire DS period, whereas QTLs emerged on chromosome 8 mostly in the late stage of DS treatment, and QTLs on chromosome 11 emerged predominantly during the early to middle stages of DS. IR-derived QTLs were mainly located on chromosomes 2, 3, 4, and 6 and RGB-derived QTLs on chromosomes 2, 3, 8, and 9. Notably, clear QTL peaks were observed near the 0- to 2-Mb region of chromosome 3 and the 4- to 6-Mb region of chromosome 8 (Figures 4B and 4C). QTLs related to multiple leaf i-traits occurred on chromosome 3 more than 800 times (QTL peak region); this was the highest frequency of QTL occurrence at the genome level, and these QTLs occurred primarily during the mid-stage of DS, suggesting that the genes in this QTL peak region might regulate leaf responses to DS. QTLs related to panicle RGB-derived i-traits occurred on chromosome 8 over 600 times, forming the QTL peak region with the second highest occurrence frequency. These QTLs occurred primarily in the mid- to late-DS stages, suggesting that the genes in this QTL peak region might modulate panicle morphology in response to DS.

Please cite this article in press as: Lou et al., Phenomics-assisted genetic dissection and molecular design of drought resistance in rice, Plant Communications (2024), https://doi.org/10.1016/j.xplc.2024.101218

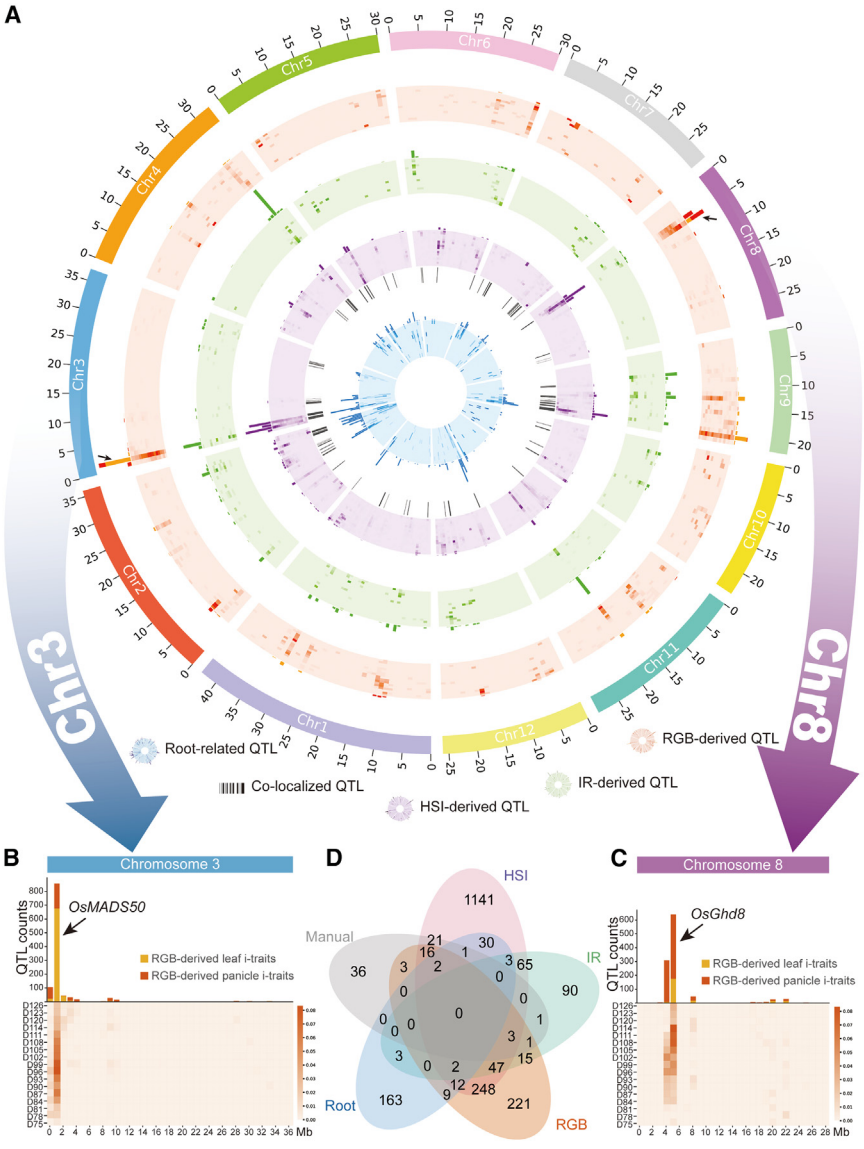

Figure 4. QTL mapping of DR-related i-traits from different sources and time points.

(A) The overall distribution of QTLs identified from DR-related i-traits. The four concentric circles, from inside to outside, represent QTLs from root-related i-traits (blue), HSI-derived i-traits (purple), IR-derived i-traits (green), and RGB-derived i-traits (orange). Black vertical lines between the blue and purple circles represent co-localized QTLs for both above- and belowground traits. Sectors of the circular diagram represent the chromosomal locations of QTLs.

(B and C) Distribution of RGB-derived QTLs on chromosome 3 **(B)** and chromosome 8 **(C)**, providing more detailed views of the regions highlighted in **(A)**. The upper section displays a histogram of QTL occurrences, where yellow bars represent QTLs related to leaf i-traits and orange bars represent QTLs related to panicle i-traits. The lower section is a heatmap showing the proportion of QTLs identified at each time point relative to the total number of QTLs, with darker colors indicating higher proportions.

(D) Venn diagram showing the numbers of QTLs identified from HSI-derived i-traits, IR-derived i-traits, RGB-derived i-traits, root-related i-traits, and manual traits, with overlapping areas indicating co-localized QTLs from different sources.

The 32 586 mapped QTLs exhibited substantial overlap among different sources of i-traits, and a total of 2097 unique QTLs were mapped. QTLs from different sources included 1591 HSI-derived aboveground QTLs, 230 IR-derived aboveground QTLs, 579 RGB-derived aboveground QTLs, and 225 RGB-derived belowground QTLs (Figure 4D). In general, aboveground QTLs from different sources exhibited a high overlap rate. Specifically, HSI-derived QTLs showed a high overlap rate with RGB-derived QTLs and IR-derived QTLs, accounting for 60.0% of all RGB-derived QTLs and 52.2% of all IR-derived QTLs. However, the overlap rate between belowground (root) and aboveground QTLs was much lower (27.6%), suggesting independent genetic DR mechanisms between aboveground and belowground systems in rice. About 57.1% of all 84 m-trait QTLs were co-localized with i-trait QTLs, providing evidence for the reliability of imaging QTL mapping.

The QTL mapping results showed that a 21.8-cM region on chromosome 8 was a region of highly dense co-localized QTLs that were mainly related to panicle i-traits and rarely to leaf i-traits (Figure 4C). The TPA_panicle_D105 trait (panicle projection area measured on day 105 after sowing) was selected as a phenotypic indicator (Figure 5A). Further analysis indicated that the LOD score of this QTL reached 9.54, and the p value between the two parental haplotypes was 2.15e−13. Bioinformatics analysis revealed that *OsGhd8*, located within this region (a 21.8-cM region on chromosome 8), has been reported to be associated with panicle morphology (Yan et al., 2011). Transcriptome analysis indicated that this gene responded to DS, exhibiting significant differences in expression between the two parental lines (Figure 5B, $p < 0.01$). The CRISPR-Cas9 technique was used to develop an *OsGhd8* knockout mutant for functional analysis. Knockout of *OsGhd8* reduced the number of primary branches in the main panicle (Figure 5C). Drought experiments performed in pots demonstrated the reduced DR of the mutant plants, as evidenced by increased curling and wilting of leaves compared with wild-type plants (Figure 5D). Under DS, the green projection area/total projection area ratio (GPAR) was significantly lower in the mutant than in the wild type, and the perimeter/projection area ratio (PAR) was significantly higher in the mutant, signifying greater leaf curling and wilting (Figure 5E, $p < 0.01$). Seed-setting percentage was also significantly lower in the mutant than in the wild type under drought treatment ($p < 0.01$). All these results suggest that the candidate gene *OsGhd8* may be a drought-responsive gene.

Please cite this article in press as: Lou et al., Phenomics-assisted genetic dissection and molecular design of drought resistance in rice, Plant Communications (2024), https://doi.org/10.1016/j.xplc.2024.101218

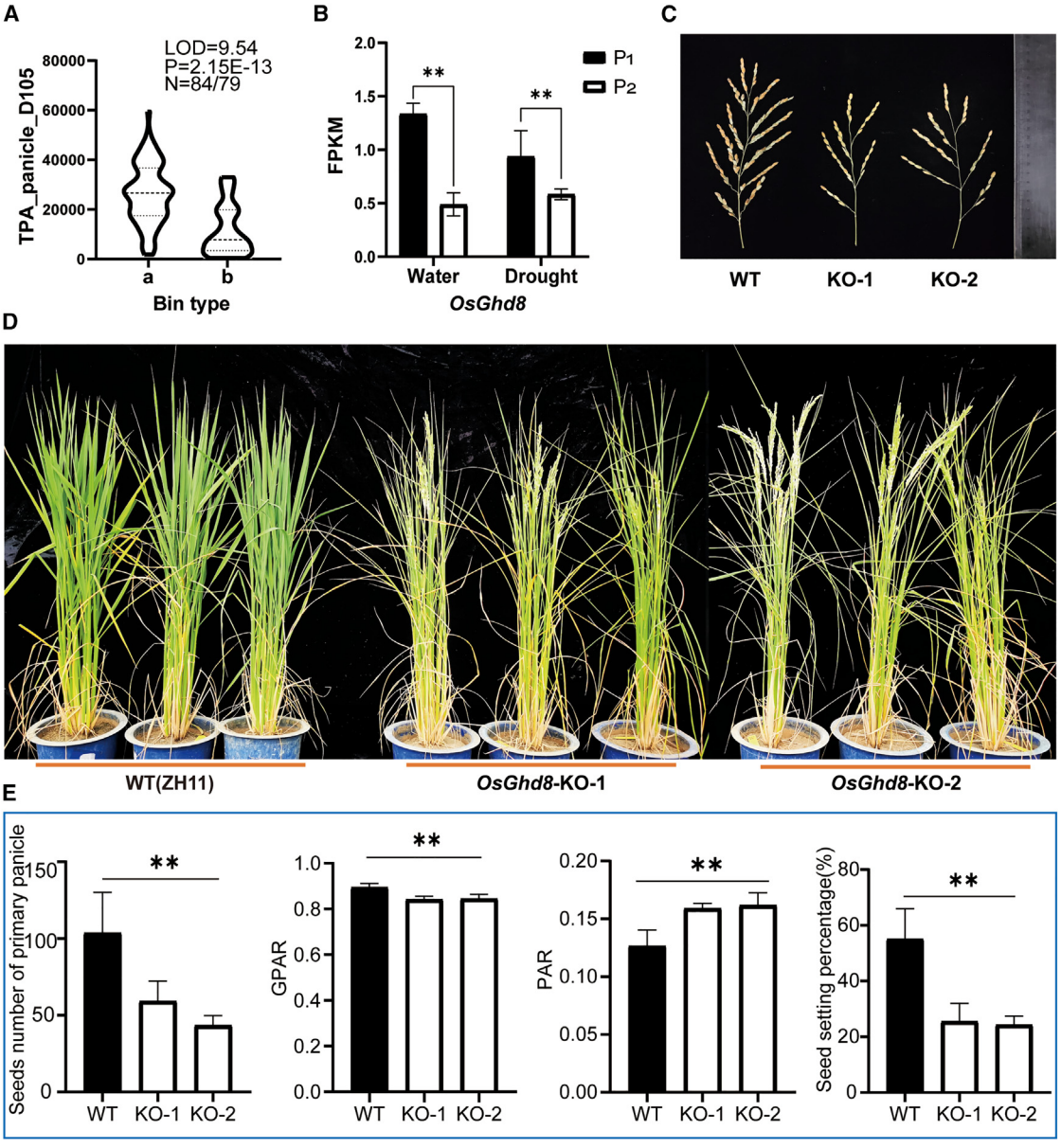

Figure 5. Verification of the DR candidate gene *OsGhd8* identified from panicle-related i-traits.

(A) Difference in panicle projection area (TPA_panicle) between two haplotypes of the candidate QTL in the population: (a) IRAT109 haplotype; (b) HH15 haplotype.

(B) Differential expression of *OsGhd8* under WW and DS treatments in the parental lines ($N = 3$). P_1, IRAT109; P_2, HH15.

(C) Morphological changes in the primary panicle of *OsGhd8*-knockout mutants.

(D) Whole-plant DR changes in *OsGhd8*-knockout mutants at day 15.

(E) Variations in four DR-related traits in mutants under drought treatment ($N = 6$).

GPAR, green projected area/total projected area ratio; PAR, perimeter/total projection area ratio. WT(ZH11), wild-type Zhonghua11 (ZH11); KO-1 and KO-2, *OsGhd8*-knockout mutants in the ZH11 background. $^*p < 0.05$, $^{**}p < 0.01$ (*t*-test).

A dense region of co-localized QTLs related to root traits was present in the middle-end region of chromosome 2 (Figure 4A). We examined a QTL related to the Mass_3_L_Ratio trait (deep-layer root length/shallow-layer root length) (Supplemental Figure 2) and found that its LOD score was 3.88 and that there was a significant difference between the two parental haplotypes ($p = 9.46e{-}05$). This QTL region contained the gene *OsSAUR11*, which has been identified as responsible for deep rooting (Xu et al., 2023). In this study, we found that *OsSAUR11* responded to DS by increasing the depth of the root system, and its knockout resulted in reduced DR, whereas its overexpression enhanced DR.

The 5′ end of chromosome 3 was another region of densely co-localized QTLs in which intense QTL genetic mapping signals were detected for aboveground and belowground i-traits from different imaging sources (Figure 4A). Interestingly, these mapped QTLs were primarily related to leaf, panicle, and root

Please cite this article in press as: Lou et al., Phenomics-assisted genetic dissection and molecular design of drought resistance in rice, Plant Communications (2024), https://doi.org/10.1016/j.xplc.2024.101218

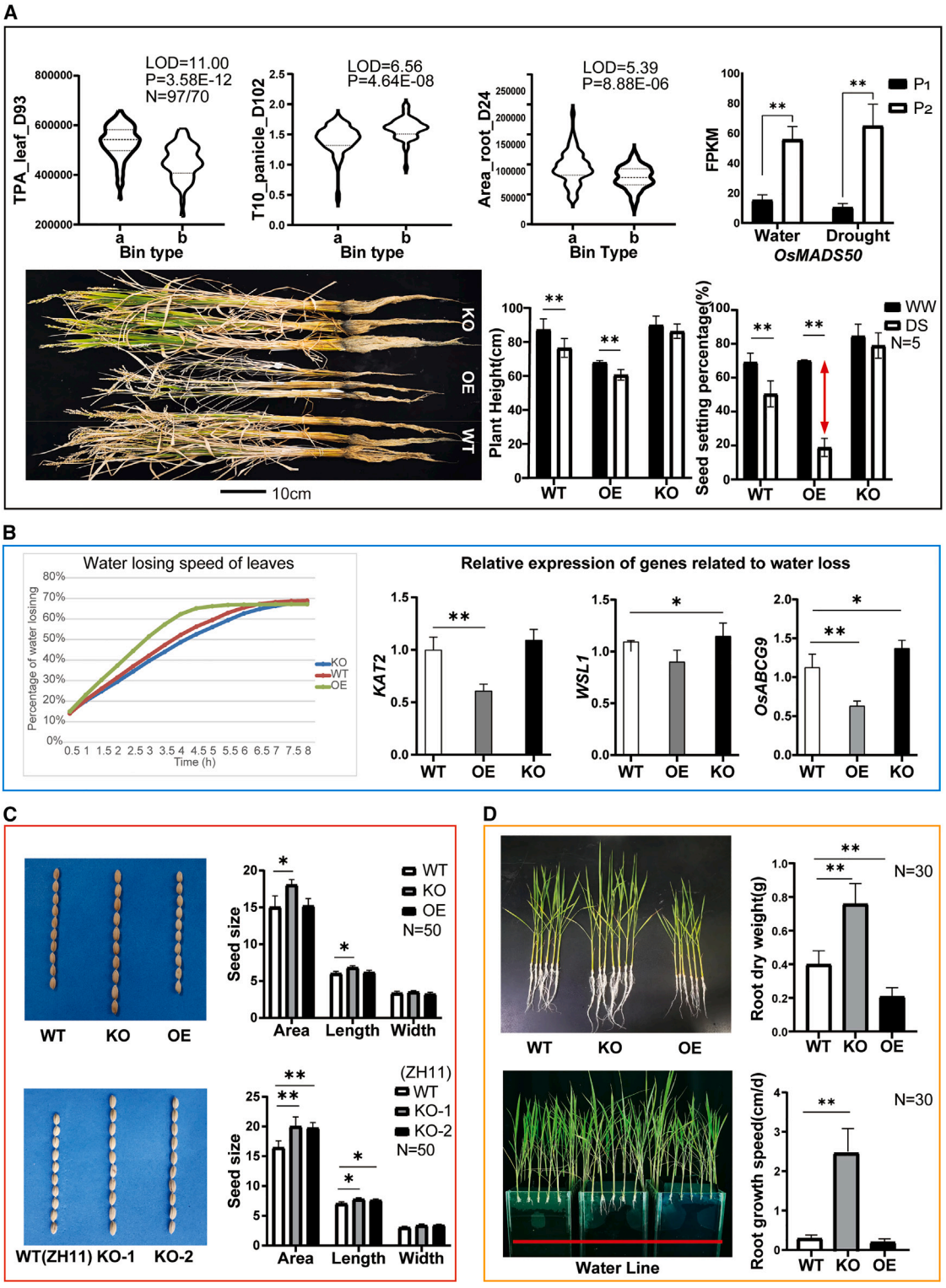

Figure 6. Functional study of the multifunctional DR candidate gene *OsMADS50*.

(A) General information on the candidate gene *OsMADS50*, including QTL mapping for leaf-related (TPA_leaf), panicle-related (T10_panicle), and root-related (Area_root) i-traits; gene expression in parental lines under WW and DS treatments ($N = 3$); and variations in plant morphology, plant height, and seed-setting percentage between WT and mutants ($N = 5$). The red double-sided arrow indicates a significant difference between the WW and DS treatment groups. P_1, IRAT109; P_2, HH15. (a) QTL haplotype of IRAT109; (b) QTL haplotype of HH15.

(B) Effect of *OsMADS50* on leaves, including changes in water-loss rate and expression of water-loss-related genes ($N = 3$).

(C) Effect of *OsMADS50* on panicles, specifically alterations in grain morphology in two mutant materials with different backgrounds ($N = 50$).

(legend continued on next page)

Please cite this article in press as: Lou et al., Phenomics-assisted genetic dissection and molecular design of drought resistance in rice, Plant Communications (2024), https://doi.org/10.1016/j.xplc.2024.101218

traits (Figure 6A). The LOD scores of QTLs related to TPA_leaf, T10_Panicle, and Area_root traits were 11.0, 6.56, and 5.39, respectively, and there was an extremely significant difference between the two parental haplotypes ($p < 0.001$). This region of co-localized QTLs included the gene *OsMADS50*, which has been reported to affect rice heading date and plant architecture (Kojima et al., 2002; Lee et al., 2004), although there have been no reports of its function in DR. Our results revealed that *OsMADS50* exhibited significantly higher expression in P_2 (HH15) than in P_1 (IRAT109) ($p < 0.001$), and it was specifically induced by drought in P_2. Further study indicated that the *OsMADS50*-overexpressing Heigeng2 (HG2) line displayed accelerated heading and reduced plant height, whereas knockout of *OsMADS50* delayed heading and increased plant height. After drought treatment, both wild-type and *OsMADS50*-overexpressing plants exhibited significantly reduced plant height and seed-setting percentage ($p < 0.001$), whereas *OsMADS50*-knockout plants showed no significant changes in plant height or seed-setting percentage before and after DS. Compared with the wild type, *OsMADS50*-overexpressing plants showed a decrease in seed-setting percentage under DS, suggesting a negative regulatory effect of this gene on DR.

Leaf water loss is closely linked to DR, and we therefore investigated the water-loss rate every half hour for 8 h (Figure 6B). The *OsMADS50*-overexpressing lines exhibited the fastest water loss from detached leaves. It took approximately 4.5 h for the *OsMADS50*-overexpressing plants to reach the highest water loss, whereas it took 7.5 h for wild-type plants and the knockout mutants. This may be one of the reasons for the lower DR of the overexpression lines. Some genes have been reported to affect stomatal closure and wax synthesis in leaves, thus increasing leaf dehydration and decreasing plant DR (Yu et al., 2008; Moon et al., 2017; Nguyen et al., 2018). The expression of three genes (*KAT2*, *WSL1*, and *OsABCG9*) was significantly reduced in the *OsMADS50*-overexpressing lines ($p < 0.05$), implying that *OsMADS50* might be involved in regulating leaf water loss. *OsMADS50*-knockout mutants in the HG2 and Zhonghua11 (ZH11) backgrounds exhibited larger grain size than wild-type plants, which may have been due primarily to an increase in grain length (Figure 6C). Knockout of *OsMADS50* resulted in improvement of DR and an increase in grain size. In addition to its effects on aboveground traits, this gene also influenced belowground traits. Compared with the wild type, the *OsMADS50*-knockout mutants showed greater root weight and length, whereas the *OsMADS50*-overexpressing plants exhibited lower root weight and length (Figure 6D). In a simulated drought experiment, the root growth rate was significantly faster in the knockout mutants than in the wild-type and overexpression plants ($p < 0.05$). The enhanced downward growth rate of roots in the knockout mutants facilitated water acquisition, thus increasing DR. Taken together, these results indicate that *OsMADS50* is a multifunctional gene that negatively regulates DR. One possible mechanism is that *OsMADS50* negatively regulates the expression of other water-loss-related genes, thus promoting dehydration, decreasing grain size, inhibiting root development, and finally decreasing plant DR.

Drought-resistance breeding guidelines

We next established yield prediction models based on i-traits by stepwise linear regression. Some i-traits exhibited good predictive capabilities for the manually measured agronomic traits (Figure 7A). The models were divided into two categories according to their predictive performance. Category I exhibited desirable predictive performance for traits of biomass, plant height, grain weight, and grain number, especially predicted by i-traits at the late drought stage ($R^{max}_{Biomass} = 0.65$, $R^{max}_{Grain\ weight} = 0.62$, Supplemental Figure 3). Category II displayed relatively weak predictive performance for traits of grain length and 1000-grain weight ($R^{max}_{Grain\ length} = 0.31$, $R^{max}_{1000-grain\ weight} = 0.38$). This may be because it is challenging to capture these fine-grain phenotypic traits from canopy images. Using these prediction models, we could predict mature-stage yield under drought conditions at the early growth stage. For example, on the basis of images captured at D96, we could accurately predict final biomass, plant height, grain weight, and grain number ($R > 0.6$) to achieve time- and labor-saving smart DR breeding.

The most critical trait for breeders is rice yield in the field under DS, including both biological and economic yield, which refer to total aboveground weight and total grain weight, respectively. We manually evaluated these two traits for 597 lines in the RIL population in Hainan province, and we developed four extreme pools (top and bottom 50 lines for each trait) with extremely high and low yields for further analysis. Through an extreme-pool-based chi-squared test, we screened more reliable DR-related QTLs from the QTLs mapped using i-traits (Figure 7B). A total of 248 QTLs related to grain weight under DS showed significantly skewed distributions between the two extreme pools ($p < 0.05$), indicating that these 248 QTLs were closely associated with economic yield under drought conditions (Supplemental Table 11). These economic-yield-related QTLs were distributed on chromosomes 1, 2, 3, 8, 9, 11, and 12, with the largest number of QTLs (68) on chromosome 8 and the second largest number (64) on chromosome 9. The majority (77.8%) of these 248 QTLs had drought-resistant alleles from P_1 (IRAT109), whereas only QTLs on chromosomes 2 and 12 had drought-resistant alleles from P_2 (HH15). Approximately 91.5% of these 248 QTLs were related to aboveground i-traits, whereas only 21 QTLs were related to belowground i-traits. Nine of the QTLs were co-localized to the 3′ end of chromosome 9 by both aboveground and belowground i-traits. A total of 272 QTLs related to the aboveground dry weight trait displayed significantly skewed distributions between the two extreme pools ($p < 0.05$), indicating that these 272 QTLs were strongly correlated with biological yield (Supplemental Table 12). These biological-yield-related QTLs were mainly distributed on chromosomes 1, 2, 3, 5, 9, and 12, with the largest number of QTLs (95) on chromosome 3 and the second largest number (72) on chromosome 9. The majority (83.1%) of these 272 QTLs had

(D) Effect of *OsMADS50* on roots, including differences in root morphology under normal watering conditions and variations in root downward growth rate under simulated drought conditions ($N = 30$). The red line represents the water level in the drought treatment.
WT, wild-type Heigeng2 (HG2); OE, *OsMADS50*-overexpressing line in the HG2 background; KO, *OsMADS50*-knockout mutant in the HG2 background; WT(ZH11), wild type of Zhonghua11 (ZH11); KO-1 and KO-2, *OsMADS50*-knockout mutants in the ZH11 background. *$p < 0.05$, **$p < 0.01$ (*t-test*).

Please cite this article in press as: Lou et al., Phenomics-assisted genetic dissection and molecular design of drought resistance in rice, Plant Communications (2024), https://doi.org/10.1016/j.xplc.2024.101218

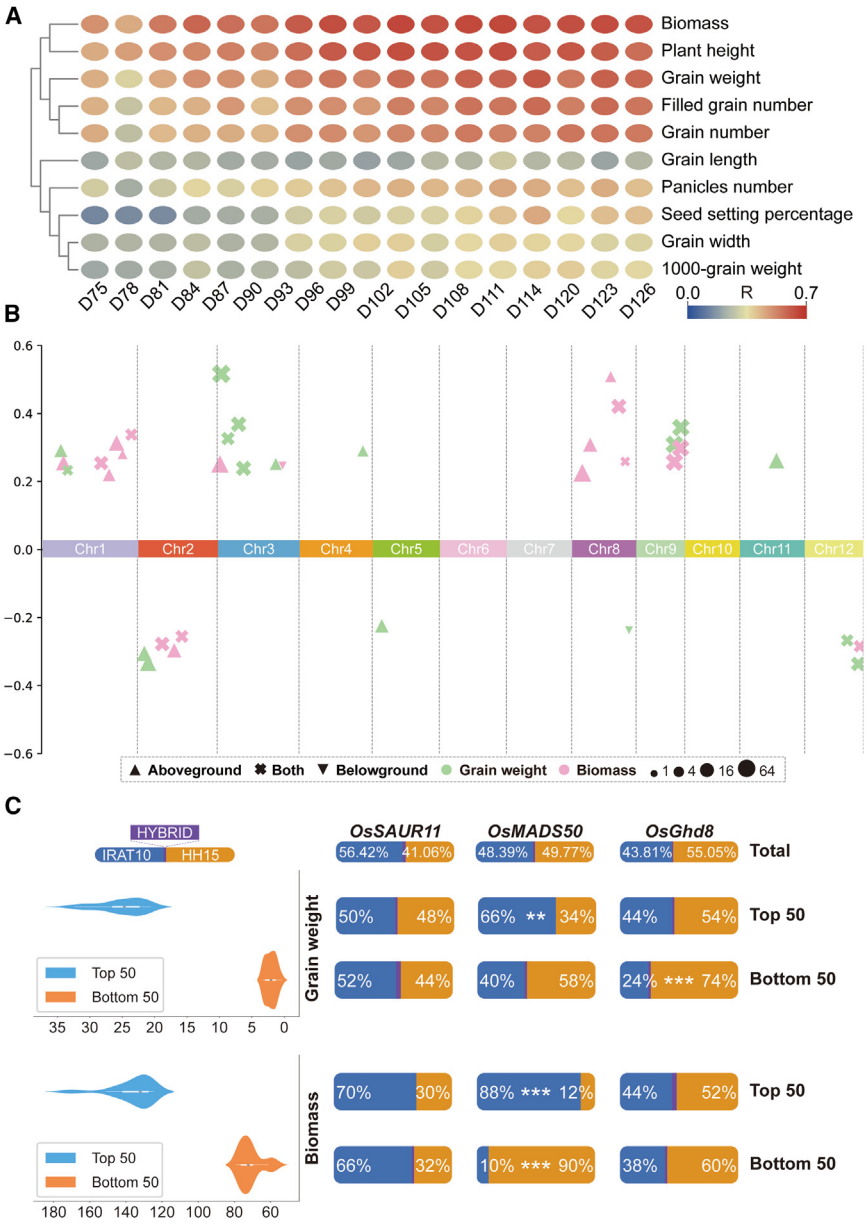

Figure 7. Breeding guidelines for improvement of drought resistance in rice.

(A) Modeling effect (*R*) of image traits on some manual traits at different time points.

(B) Distribution of composite QTLs screened by chi-squared tests of grain weight and biomass under DS treatment. The *x* axis shows the genomic positions of the QTLs; the *y* axis indicates the allele frequency difference between the extreme pools. A positive value means that the alleles from P_1 (IRAT109) are superior DR alleles, whereas a negative value means that the P_2 (HH15) alleles are superior. Different shapes indicate different sources of QTLs: upright triangles indicate QTLs that come from aboveground traits; crosses indicate QTLs that were detected from both belowground and aboveground traits; inverted triangles indicate QTLs that come from belowground traits. QTLs related to grain weight are colored green, and QTLs related to biomass weight are colored pink. The size of the symbol indicates the number of QTLs converged in this composite QTL region.

(C) Allele analysis of three drought-resistant genes in extreme pools for grain weight and biomass. Blue indicates the IRAT109 allele, orange indicates the HH15 allele, purple indicates the hybrid allele type of the parents, and the number in columns indicates the percentage of alleles. "Total" refers to the entire subpopulation of 597 RIL lines evaluated in the field in Hainan province; "Top 50" indicates the 50 lines with the highest grain weight or biomass; "Bottom 50" indicates the 50 lines with the lowest grain weight or biomass. The violin diagram on the left shows the grain weight and biomass distribution of the top and bottom lines. $^{**}p < 0.01$, $^{***}p < 0.001$ (chi-squared test, $N = 50$).

drought-resistant alleles from P_1, whereas only QTLs on chromosomes 2, 8, and 12 exhibited drought-resistant haplotypes from P_2. About 83.1% (226) of these 272 QTLs were primarily related to aboveground i-traits; only 46 were related to belowground i-traits, and 11 QTLs were co-localized by aboveground and belowground i-traits. There were more belowground biological-yield-related QTLs (46) than belowground economic-yield-related QTLs (21), suggesting that belowground traits play an important role in improving biomass under DS. The QTLs co-localized by both aboveground and belowground traits deserve more attention in future studies. Figure 7B shows the key QTLs with their related traits and contribution directions, providing valuable guidance for the improvement of DR traits and drought-resistant rice breeding.

We also analyzed the haplotype distribution of the three DR genes identified in this study. Figure 7C illustrates the haplotype percentages of the three DR genes in the extreme pools for the yield trait. The distribution frequency of the two haplotypes of the drought candidate gene *OsSAUR11* related to root traits in the whole population (597 lines) was 56.42% for P_1 and 41.06% for P_2. No significantly skewed distribution was detected in the extreme pools for grain weight and aboveground dry weight (biomass) traits, indicating no significant contribution of this root-related gene to grain yield and biomass traits, perhaps because of the limited effect of roots in the clay soil conditions of Hainan province. The haplotype frequency ratio of the multi-effect DR gene *OsMADS50* from the two parent lines in the whole population was nearly 1:1. In the top-50 pools of grain weight and aboveground biomass traits, the P_1 haplotype was dominant over the P_2 haplotype ($p < 0.05$), whereas in the bottom-50 pool of the aboveground biomass trait, the P_2 haplotype was overwhelmingly dominant (90%) over the P_1 haplotype. This suggested that the P_1 haplotype of this gene was superior to the P_2 haplotype for DR. It is therefore advisable to introduce the P_1 haplotype and minimize the P_2 haplotype to improve grain weight or biomass in DR breeding through molecular design. Supplemental Figure 4 presents the molecular

Please cite this article in press as: Lou et al., Phenomics-assisted genetic dissection and molecular design of drought resistance in rice, Plant Communications (2024), https://doi.org/10.1016/j.xplc.2024.101218

clustering of three DR-related genes in the genomes of 20 rice varieties. The genes of IRAT109 (P_1) were distant from those of other varieties, forming an independent cluster. This distinctive haplotype of IRAT109 might be a rare and valuable genetic resource for DR breeding. In this regard, only the HH15 (P_2) haplotype of the DR gene *OsGhd8*, which controls panicle traits, was significantly enriched in the bottom-50 pool of the grain-weight trait ($p < 0.01$). This result indicates a negative regulatory effect of the P_2 haplotype on grain weight, and introduction of the P_2 haplotype of *OsGhd8* should therefore be minimized in DR breeding. The molecular evolutionary tree also showed that *OsGhd8* from the rice variety OSPr106 was identical to that from HH15 (P_2), suggesting that the haplotype of the HH15-like variety should be avoided as a genetic resource, especially in DR breeding (Supplemental Figure 4).

DISCUSSION

In this study, we used HTPPs to obtain dynamic phenomic data for 217 rice lines in the field and in root boxes under drought and non-drought conditions by multimodal imaging. We constructed a linkage map of drought-resistant rice varieties that contained a large number of QTLs (32 586) localized by extremely abundant i-traits (139 040). The abundant and comprehensive i-traits and the corresponding QTLs obtained in this experiment can serve as a rich resource for the breeding of drought-resistant rice varieties. Furthermore, compared with pot-based drought treatments (Chen et al., 2014; Guo et al., 2018; Wu et al., 2021), the DS progression in our field experiment was slower and milder and thus much closer to the real scenario of DS in actual rice production. The aboveground i-traits captured by the HTPP from Shanghai and the manually measured m-traits from Shanghai and Hainan were all obtained from field experiments, rendering our experimental results more reliable and applicable to actual breeding practices.

Compared with the IRAT109 genome (377 Mbp, 305 gaps) released by Wang et al. (2024), our assembled genome (384 Mbp, 77 gaps) was slightly longer and had many fewer gaps (Supplemental Figure 5). In addition to the centromere region, chromosomes 1, 6, 9, and 11 also differed in the two versions of the IRAT109 genome. Unlike conventional genome assembly, this study used a linkage map as the skeleton to assist in assembly and integrated a proteogenomic database to improve gene annotation, thus obtaining a high-quality genome. Only 35 066 genes were annotated in the previously reported IRAT109 genome, whereas 55 498 genes were annotated in our IRAT109 genome. We also assembled and released a high-quality genome of HH15, the first genome of a typical drought-tolerant rice, with a total of 61 947 annotated genes. By analyzing the collinearity among IRAT109, HH15, and 16 previously published rice genomes, we identified 9209 genes specific to the typical DA variety IRAT109 and 14 584 genes specific to the DT variety HH15 (Supplemental Tables 3 and 4). All these findings will be useful for genetic dissection and DR breeding.

We used multimodal cameras for continuous data collection at 17 time points and obtained a vast dataset (with about 4 Tb of imaging data). Data processing and feature extraction posed a significant challenge. To address this challenge, we established an automatic image-processing pipeline (Supplemental Video 1), and the images captured by various multimodal (HSI, IR, and RGB) cameras enabled the analysis of complicated traits such as DR. Moreover, selection of a suitable time for i-trait collection is very important, because the heritability and the effects of QTL mapping and model prediction are closely related to plant growth stage. For example, leaf traits tend to appear earlier than panicle traits; hence, data collection for leaf traits should be preceded by that for panicle traits. Furthermore, we constructed prediction models to predict m-traits on the basis of i-traits at the early growth stage. Overall, this study provides a valuable reference for multimodal time-series phenomic analyses of complex traits.

We used an extreme-pool-based QTL screening method to screen numerous QTLs as an intermediate product (Figure 7B). The skewed distribution of QTL peaks exhibited a regional and continuous pattern, enabling the QTLs to be clustered into a smaller number of composite QTLs on the basis of linkage distance, contributing to their practical application in breeding (Supplemental Tables 11 and 12). A total of 18 composite QTLs related to the grain-weight trait and 21 composite QTLs related to the biomass trait were obtained by merging adjacent QTLs based on a genetic distance of 3 cM. A total of 33 and 52 known genes related to rice DR were captured, respectively, by the composite QTLs for grain weight and biomass. Twelve known genes were captured by the QTLs for both grain and biomass traits, including *DSM2*, *HYR*, *OMTN3*, *ONAC022*, *Os9BGlu33*, *OsCDPK1*, *OsDREB1A*, *OsDSG1*, *OsHB22*, *Oshox4*, *OsRF1*, and *OsSAP1* (Dubouzet et al., 2003; Du et al., 2010; Park et al., 2010; Giri et al., 2011; Chen et al., 2012; Ho et al., 2013; Ambavaram et al., 2014; Fang et al., 2014; Ren et al., 2019; Zhou et al., 2020; Kim et al., 2021; Yang et al., 2022a). These composite QTLs can be used directly for future marker-assisted selection during breeding. Yield-related QTLs were predominantly distributed on chromosomes 8 and 9, whereas biomass-related QTLs were mainly found on chromosomes 3 and 9. Alleles that improved yield and biomass under DS were derived mainly from the IRAT109 parent. Therefore, the DA rice variety IRAT109 might be an excellent genetic resource for DR breeding.

It is crucial to select different combinations of haplotypes according to various environments and objectives for molecular-design breeding. Different DR traits need to be considered for environment-specific breeding. For instance, in upland environments, a deep-rooting-related drought-avoidance trait is more crucial than other traits, because growth in uplands requires roots to grow deeper to absorb water from deeper soil layers. Therefore, DR QTLs related to root traits should be considered for upland rice breeding. The clay soil environment is unfavorable to root penetration; thus, the DT of aboveground parts becomes pivotal, and DR QTLs associated with aboveground traits should be considered. In addition, different breeding objectives necessitate distinct genetic loci. For example, in breeding aimed at increasing grain yield under DS, great emphasis should be placed on QTLs that control grain, such as QTLs on chromosome 8 in this study. By contrast, when breeding for forage purposes, QTLs on chromosomes 1 and 3 that enhance aboveground biomass should be given preference. Moreover, the QTL region at the 3′ end of chromosome 9 was consistently found to be related to both economic and biological yield traits, indicating that this QTL region has great application potential for future DR breeding.

Please cite this article in press as: Lou et al., Phenomics-assisted genetic dissection and molecular design of drought resistance in rice, Plant Communications (2024), https://doi.org/10.1016/j.xplc.2024.101218

METHODS

Materials

IRAT109 is a typical upland rice variety developed and first released in Cote d'Ivoire. Hanhui15 (HH15) is a WDR restorer line developed by SAGC. The RIL population with 1500 lines was developed by crossing IRAT109 with HH15 and self-crossing from the F_2 to the F_8 generation via an SSD method. The genome resequencing data for 1262 lines were used to construct the linkage map, and 217 lines that differed in growth duration by <10 days were used for phenotypic scanning on the HTPP. Five hundred ninety seven lines from the RIL population (out of 1262 lines and not used in the aforementioned HTPP) were grown during the dry season with three biological replicates in Hainan, China, to measure their total aboveground weight and total grain weight in the field under natural drought conditions.

An *OsGhd8* knockout mutant was obtained by the CRISPR-Cas9 technique in the ZH11 background. A knockout mutant of *OsSAUR11* was generated in the IRAT109 background, and a mutant overexpressing *OsSAUR11* was developed in the Nipponbare background (Xu et al., 2023). *OsMADS50* knockout and overexpression mutants in the HG2 background were provided by Professor Chuanzao Mao's laboratory in Zhejiang University, China (Shao et al., 2019). Another *OsMADS50* knockout mutant in the ZH11 background was purchased from BIOGLE GeneTech (Hangzhou, China). The sequence information for the three candidate genes in the parent lines is shown in Supplemental Table 13, and the sequence information for the transgenic/mutant materials is shown in Supplemental Figure 6.

Genome sequencing and *de novo* assembly

The gDNA samples of the parents (IRAT109 as P_1 and HH15 as P_2) were sequenced by NRGENE using Illumina second-generation sequencing with a total coverage depth of 319× and 279× in 2018. Accurate raw data were obtained from paired-end and mate-pair libraries. Third-generation sequencing libraries were also prepared, and the parent samples were sequenced to obtain additional sequencing data with a coverage depth of 44× for P_1 and 40× for P_2. About 28 Gb of PacBio HiFi reads (with a coverage depth of 70× and average sub-read length of 15 092 bp) from the HH15 variety were obtained to assemble the genome. The genomes of IRAT109 and HH15 were assembled *de novo,* using the genetic map of the RIL population derived from these two parents as the skeleton. The assembly procedures were as follows. First, the heterozygosity of the genomes was estimated using Jellyfish v.2.2.6 (k-mer analysis) and GenomeScope 1.0 software. Second, reads were assembled into contigs using Hifiasm (v.0.16.1-r375), Canu (v.2.1.1), Falcon (v.1.8.4), and Flye (v.2.9) software. Third, the contigs were assembled into pseudo-chromosomes using Genome Puzzle Master, with MH63RS3 as the reference (Song et al., 2021a). Finally, chromosome sequences were polished using Racon (v.1.3.3) to improve single-base quality. The whole proteome of multiple organs of IRAT109 at different developmental stages under non-drought and drought conditions was developed as reported previously (Yang et al., 2014), then used to construct a proteomic database to minimize possible errors in the genome assembly and improve the IRAT109 genome annotation. On the basis of the transcriptome and proteome data, the genome was annotated using MAKER software, and more than 50 000 genes were annotated in each of the HH15 and IRAT109 genomes. The sequence collinearity of the two genomes was then compared using MUMmer software. Furthermore, some genes specific to the HH15 (DA variety) and IRAT109 (DT variety) genomes were compared with those in 17 other rice variety genomes in the Rice Gene Index database (Yu et al., 2023).

Sequencing of the RIL population and construction of a genetic map

DNA was extracted from leaf samples collected from a single plant of each RIL in April 2020 for library construction. Whole-genome paired-end resequencing was performed on the Illumina NovaSeq platform with an average genomic coverage of 5×. SNP loci were identified and filtered using UnifiedGenotyper with a stand_call_conf of 30 and a stand_emit_conf of 10. A total of 11 785 bin markers were identified by the Bayesian algorithm with the parameters frequency >0.3, heterozygosity <0.2, and distance >200 bp. A linkage map with a total length of 1151.7 cM was developed based on linkage groups of bins determined using "onemap" and marker ordering within linkage groups based on the Kosambi algorithm (Margarido et al., 2007).

Drought treatment and aboveground phenomic data collection by HTPP

In the summer of 2021, phenotypic data for 217 lines from the RIL population that differed in growth duration by <10 days were collected under gradient water scenarios on the HTPP specialized for DR at Jinshan Experimental Farm of the SAGC (Langxia, Jinshan, Shanghai; 121.2°E, 30.8°N). Similar to the method used in our previous drought screening facility (Liu et al., 2006), the plot (6.8 m in total length), known as the "drought screening island," was divided by a middle shallow ditch (about 30 cm in depth, serving as the water supplier) into two back-to-back subplots with a length of nearly 3 m each, enabling soil water gradients through infiltration irrigation, and there was a deep drainage channel (2 m in depth) along both sides of the plot. Rice seeds were sown in the nursery at the end of May 2021, and seedlings were then transplanted to the HTPP at the end of June. Each subplot had four rows with 16 plants per row, 20 cm between rows, and 18 cm between plants, following a randomized block design with three replicates. After 1 month of normal growth (under non-drought conditions), irrigation was stopped, and the water level in the drainage channel was decreased to about 1.8 m below the soil surface. Only in the middle water ditch was a water layer of about 15 cm maintained by infiltration irrigation for about 45 days, after which full irrigation was restored at the stage of rice grain filling and maturation. After irrigation was stopped, rice plants located near the drainage channels suffered from increasing water-deficit stress, i.e., they were under DS treatment, whereas a normal water level was maintained for rice plants near the middle water ditch, i.e., they were under WW treatment. For plants under the DS and WW treatments, all environmental factors except soil moisture were identical, enabling the comparison of plant DR under DS and WW treatments.

A gantry moving system (sensor to plant) carrying multimodal imaging devices including HSI, IR, and RGB cameras was set up as one part of the aboveground HTPP. All plots were scanned once every 3 days from day 75 post sowing (D75), and hyperspectral and visible-light imaging was performed from 19:00 h to 05:00 h the next day, with infrared imaging from 14:00 h to 17:00 h. From D75 to D126, 17 instances of image acquisition were performed, with one missing on D117. Five representative plants with uniform growth status were selected from the DS and WW regions of each subplot for manual measurement of traits including plant height, plant tiller number, aboveground biomass (dry weight), panicle number, grain dry weight, seed-setting percentage, and 1000-grain weight at the maturing stage.

Development of predictive models

Predictive models were developed by stepwise linear regression, with the i-traits of aboveground parts obtained at each time point as independent variables and the m-traits as dependent variables. The dataset was split into training and test sets using a 5-fold cross-validation method. The model was trained and tested 100 times, and the average correlation coefficient (R) on the test set was used to evaluate the effectiveness of the model.

Drought treatment and belowground phenomic data collection from root boxes

The phenotypic data for belowground parts were collected from the same population used for aboveground part examination in autumn 2022 in

Please cite this article in press as: Lou et al., Phenomics-assisted genetic dissection and molecular design of drought resistance in rice, Plant Communications (2024), https://doi.org/10.1016/j.xplc.2024.101218

Wuhan. The root boxes (30 cm width × 50 cm depth) were arrayed side by side with an inclination angle from the ground. Root-system images were captured by high-resolution visible-light cameras carried by a small rail vehicle in sensor-to-plant mode. Seeds were sown atop each root box with six replicates per line. Full irrigation was initially applied to all root boxes. Irrigation was stopped for half of the root boxes at day 21 post sowing (D21) to enable the development of DS, while the other half of the root boxes were well watered. Beginning on the date of irrigation termination (D21), visible-light imaging of all root boxes was performed once every 3 days, from 07:00 h to 22:00 h (in total, nine time points from D21 to D45). Finally, the lengths and weights of whole plants and roots were measured manually.

Manual acquisition of yield traits for 597 unused lines (out of 1262) in the field

Five hundred ninety-seven lines with a similar heading date in the RIL population from Hainan province were selected for manual investigation of DR. The field experiments were performed from December 2021 to May 2022 during the dry season at the Shanghai Nanfan Experimental Station. Each plot consisted of 5 rows × 7 plants, with three replicates for each line. After 2 months of normal growth, drought treatment was initiated by stopping watering, and watering was then restored 1 month later. Five plants with uniform growth status from each subplot were harvested at the mature stage to measure their biomass and grain weight.

Drought treatment of mutant materials in pots for phenotyping

Phenotypes of the three candidate gene mutants were investigated in Wuhan by pot drought experiments. In mid-May 2023, seedlings at the two-leaf stage were transferred to pots (20 cm in diameter and 18 cm in depth). There were 12 replicates for each line. After 60 days of normal growth, the plants were moved to a greenhouse for drought experiments. The pots were weighed daily from day 10 post watering termination. According to the measured weight, water was added to maintain 15% relative soil moisture. After 10 days of treatment, pots were moved to an imaging darkroom and photographed every 2 days to obtain i-traits such as TPA (total projected area), GPAR, and PAR. After a 20-day drought treatment, plants were rewatered at the mature stage, and their aboveground parts were harvested for manual measurement of yield traits to obtain m-traits such as panicle number, grain number per panicle, grain weight, grain size, and seed-setting percentage.

Drought-stress simulation in root chambers and phenotyping

In June 2023, seeds were germinated at 30°C for 2 days. Uniformly germinated seeds were sown into open-bottomed 96-well PCR plates and grown in a nutrient solution for 14 days. Seedlings with uniform growth status were selected, and their roots were trimmed to 0.5 cm and placed into root chambers (14 cm length, 14 cm width, 28 cm depth) (Figure 6D). The root of each seedling was positioned at the same height between the black filter paper and the transparent chamber wall. Nutrient solution was added to the chamber (10 cm below the roots), thus maintaining a certain humidity near the roots through the filter paper. This system was designed to simulate DS, ensuring that the roots were not saturated with water, while maintaining a certain level of humidity. Each side wall of one chamber accommodated five seedlings, with 30 replicates for each line. After initial trimming, root lengths were measured every day to evaluate root growth rate.

Environmental data collection

One hundred water potential sensors were evenly installed in the field of the HTPP before drought treatment to monitor changes in soil water potential at a depth of 15 cm from the soil surface. Two meteorological stations were installed, one inside and one outside the greenhouse of the HTPP, to monitor meteorological parameters such as air temperature, humidity, and light intensity. All data were measured automatically and automatically saved every hour.

Phenotypic trait screening

First, three replicates of all the i-traits from the DS and WW treatments and their mean values were obtained for subsequent analysis. Second, the 3σ rule was used to eliminate outliers. A two-sample equal-variance *t*-test was performed to assess the differences between the WW and DS treatments. Only traits with a confidence interval >95% were selected for subsequent genetic analysis. The broad-sense heritability for i-traits at different time points was calculated according to the following formula.

$$H_b = \frac{\hat{\sigma}_g^2}{\hat{\sigma}_g^2 + \hat{\sigma}_e^2} = \frac{V_1 - V_2}{V_1 + (r-1)V_2},$$

where V_1 represents the between-group variance; V_2 denotes the within-group variance; and r is the number of replicates. Only traits with a heritability >0.1 were retained for subsequent genetic analysis.

QTL mapping

Genetic mapping of phenotypic traits was performed to identify major-effect QTLs. The genetic distance was calculated by the Kosambi method in the CIM function of R/qtl software (Peñuelas et al., 1997). The Haley–Knott method was used for QTL scanning. QTLs with an LOD score >2.5 were considered to be candidate QTLs and used for subsequent analyses. A span of 150 kb on either side of the SNP with the highest LOD in the QTL was defined as the QTL region. Adjacent QTLs whose 150-kb span regions overlapped were designated composite QTLs.

Transcriptomes of parental lines under water-deficit conditions

In the summer of 2022, after 70 days of growth under normal conditions, potted plants of the IRAT109 and HH15 parental lines were subjected to a 10-day drought treatment (Supplemental Figure 1C). Five leaves were collected from potted plants for transcriptome sequencing, with three replicates of each line and treatment. Transcriptome sequencing was performed by Shanghai Majorbio Bio-pharm Technology (Shanghai, China) following standard procedures for RNA extraction, reverse transcription, library construction, and sequencing. Transcriptome information for the DR-related genes in the parental lines is provided in Supplemental Table 14.

Gene-expression quantification

The expression levels of target genes were detected by qPCR using the TransStart Top Green qPCR Supermix kit (Transgene) and the CFX96 real-time PCR system (Bio-Rad). Gene expression was calculated using the $2^{-\Delta\Delta Ct}$ method and normalized using the rice actin gene *OsACT2* as the reference gene. The nucleic acid sequences of primers used in qPCR were:

KAT2F: CGA GTT GCA GTC CTG TAG TT; KAT2R: TCC ACA GAT CAT AGA GGG C;

WSL1F: GGT TGC CAA GAA GGT CCT CA; WSL2R: TGT GCC AGT CAG TCA ACT CC;

ABCG9F: CAC CCA GGT TTC TCC CAC TA; ABCG9R: GCT TCG GAA TGT CGT AAG GA.

Leaf dehydration rate

After approximately 60 days of normal growth, leaves were collected from plants. Leaves were cut into segments (10 cm in length) and placed in a 25°C environment for natural dehydration. To measure leaf dehydration rate, the weight of five leaves from each replicate was measured every half hour from 0 to 8 h post collection, with five replicates for each line.

i-Trait QTLs screened by chi-squared test

On the basis of the experiment results from Hainan province, we established extreme pools containing the top and bottom 50 lines for aboveground biomass and grain yield. A chi-squared test was performed to

Please cite this article in press as: Lou et al., Phenomics-assisted genetic dissection and molecular design of drought resistance in rice, Plant Communications (2024), https://doi.org/10.1016/j.xplc.2024.101218

screen QTLs with a significantly skewed distribution between the two parental alleles and for which these two parental allele frequency differences were >0.2 between the top and bottom pools. The i-trait QTLs screened according to biomass or grain yield under DS from the validated subpopulation may be promising loci for use in drought-resistant rice breeding. A similar chi-squared test was performed for three candidate genes.

DATA AND CODE AVAILABILITY

All the phenome data and core data-handling code have been deposited online.

Genome data

https://riceome.hzau.edu.cn/download.html.

Aboveground data

http://plantphenomics.hzau.edu.cn/usercrop/Rice/image/2021-JinshanAboveground.

Belowground data

http://plantphenomics.hzau.edu.cn/usercrop/Rice/image/2022-WuhanUnderground.

Project home page

https://github.com/Crystalysafer/Rice-Drought-program.

Deep-learning model and GUI

https://github.com/Crystalysafer/Rice-Drought-program/releases/tag/V1.0.

FUNDING

This research was supported by the National Natural Science Foundation of China (32172098 and U21A20205) and the Natural Science Foundation of Shanghai (23ZR1455900 and 22ZR1455200).

ACKNOWLEDGMENTS

No conflict of interest declared.

AUTHOR CONTRIBUTIONS

Conceptualization, Q.L. and L.L.; software, Y.C. and F.L.; formal analysis, Y.C.; investigation, Q.L., Y.C., X.W., Y.Z., T.G., J.S., M.Y., F.F., K.X., S.X., X.X., W.L., Y.N., H.G., H.X., L.W., T.L., S.C., Y.Z., and J.Z.; resources, H.M. and L.L.; data curation, Y.C.; writing – original draft, Q.L., Y.C., and X.W.; writing – review & editing, Q.L., Y.C., X.W., and H.M.; visualization, Y.C.; supervision, W.Y. and L.L.; project administration, L.C.; funding acquisition, Q.L.

SUPPLEMENTAL INFORMATION

Supplemental information is available at *Plant Communications Online*.

Received: September 15, 2024
Revised: November 16, 2024
Accepted: December 4, 2024

REFERENCES

Ambavaram, M.M.R., Basu, S., Krishnan, A., Ramegowda, V., Batlang, U., Rahman, L., Baisakh, N., and Pereira, A. (2014). Coordinated regulation of photosynthesis in rice increases yield and tolerance to environmental stress. Nat. Commun. **5**:5302.

Araus, J.L., Kefauver, S.C., Zaman-Allah, M., Olsen, M.S., and Cairns, J.E. (2018). Translating High-Throughput Phenotyping into Genetic Gain. Trends Plant Sci. **23**:451–466.

Bhandari, U., Gajurel, A., Khadka, B., Thapa, I., Chand, I., Bhatta, D., Poudel, A., Pandey, M., Shrestha, S., and Shrestha, J. (2023). Heliyon Morpho-physiological and biochemical response of rice (*Oryza sativa L.*) to drought stress : A review. Heliyon **9**:e13744.

Blum, A. (2010). Plant breeding for water-limited environments (Springer Science & Business Media).

Briglia, N., Williams, K., Wu, D., Li, Y., Tao, S., Corke, F., Montanaro, G., Petrozza, A., Amato, D., Cellini, F., et al. (2020). Image-based assessment of drought response in grapevines. Front. Plant Sci. **11**:595.

Champoux, M.C., Wang, G., Sarkarung, S., Mackill, D.J., O'Toole, J.C., Huang, N., and McCouch, S.R. (1995). Locating genes associated with root morphology and drought avoidance in rice via linkage to molecular markers. Theor. Appl. Genet. **90**:969–981.

Chen, D., Neumann, K., Friedel, S., Kilian, B., Chen, M., Altmann, T., and Klukas, C. (2014). Dissecting the phenotypic components of crop plant growth and drought responses based on high-throughput image analysis. Plant Cell **26**:4636–4655.

Chen, F., Shi, X., Chen, L., Dai, M., Zhou, Z., Shen, Y., Li, J., Li, G., Wei, N., and Deng, X.W. (2012). Phosphorylation of FAR-RED ELONGATED HYPOCOTYL1 is a key mechanism defining signaling dynamics of phytochrome a under red and far-red light in *Arabidopsis*. Plant Cell **24**:1907–1920.

Du, H., Wang, N., Cui, F., Li, X., Xiao, J., and Xiong, L. (2010). Characterization of the β-carotene hydroxylase gene DSM2 conferring drought and oxidative stress resistance by increasing xanthophylls and abscisic acid synthesis in rice. Plant Physiol. **154**:1304–1318.

Dubouzet, J.G., Sakuma, Y., Ito, Y., Kasuga, M., Dubouzet, E.G., Miura, S., Seki, M., Shinozaki, K., and Yamaguchi-Shinozaki, K. (2003). OsDREB genes in rice, Oryza sativa L., encode transcription activators that function in drought-high-salt- and cold-responsive gene expression. Plant J. **33**:751–763.

Fang, Y., Xie, K., and Xiong, L. (2014). Conserved miR164-targeted NAC genes negatively regulate drought resistance in rice. J. Exp. Bot. **65**:2119–2135.

Giri, J., Vij, S., Dansana, P.K., and Tyagi, A.K. (2011). Rice A20/AN1 zinc-finger containing stress-associated proteins (SAP1/11) and a receptor-like cytoplasmic kinase (OsRLCK253) interact via A20 zinc-finger and confer abiotic stress tolerance in transgenic *Arabidopsis* plants. New Phytol. **191**:721–732.

Fukao, T., and Xiong, L. (2013). Genetic mechanisms conferring adaptation to submergence and drought in rice: simple or complex? Current opinion in plant biology **16**:196–204.

Gao, H., Xu, X.-y., Chen, Y.-y., Liu, H.-y., Chen, L., Yang, W.-n., Luo, L.-j., and Lou, Q.-j. (2022a). Construction and application of the high throughput phenomics platform for water-saving and drought-resistance rice (WDR). Acta Agriculturae Shanghai **38**:46–55.

Guo, Z., Yang, W., Chang, Y., Ma, X., Tu, H., Xiong, F., Jiang, N., Feng, H., Huang, C., Yang, P., et al. (2018). Genome-wide association studies of image traits reveal genetic architecture of drought resistance in rice. Mol. Plant **11**:789–805.

Ho, S.L., Huang, L.F., Lu, C.A., He, S.L., Wang, C.C., Yu, S.P., Chen, J., and Yu, S.M. (2013). Sugar starvation- and GA-inducible calcium-dependent protein kinase 1 feedback regulates GA biosynthesis and activates a 14-3-3 protein to confer drought tolerance in rice seedlings. Plant Mol. Biol. **81**:347–361.

Houle, D., Govindaraju, D.R., and Omholt, S. (2010). Phenomics: the next challenge. Nat. Rev. Genet. **11**:855–866.

Gao, H., Xu, X.Y., Chen, Y.Y., Liu, H.Y., Chen, L., Yang, W.N., Luo, L.L., and Lou, Q.J. (2022b). Construction and application of the high

throughput phenomics platform for water-saving and drought-resistance rice(WDR). Acta Agric. **38**:46–55.

Khowaja, F.S., and Price, A.H. (2008). QTL mapping rolling, stomatal conductance and dimension traits of excised leaves in the Bala × Azucena recombinant inbred population of rice. Field Crops Res. **106**:248–257.

Kim, S., Park, S.I., Kwon, H., Cho, M.H., Kim, B.G., Chung, J.H., Nam, M.H., Song, J.S., Kim, K.H., and Yoon, I.S. (2021). The Rice Abscisic Acid-Responsive RING Finger E3 Ligase OsRF1 Targets OsPP2C09 for Degradation and Confers Drought and Salinity Tolerance in Rice. Front. Plant Sci. **12**:797940.

Kim, Y., Chung, Y.S., Lee, E., Tripathi, P., Heo, S., and Kim, K.H. (2020). Root Response to Drought Stress in Rice (Oryza sativa L .). Int. J. Mol. Sci. **21**:1513.

Kojima, S., Takahashi, Y., Kobayashi, Y., Monna, L., Sasaki, T., Araki, T., and Yano, M. (2002). Hd3a, a rice ortholog of the *Arabidopsis* FT gene, promotes transition to flowering downstream of Hd1 under short-day conditions. Plant Cell Physiol. **43**:1096–1105.

Lee, S., Kim, J., Han, J.J., Han, M.J., and An, G. (2004). Functional analyses of the flowering time gene OsMADS50, the putative Suppressor of Overexpression of CO 1/Agamous-Like 20 (SOC1/AGL20) ortholog in rice. Plant J. **38**:754–764.

Li, B., Chen, L., Sun, W., Wu, D., Wang, M., Yu, Y., Chen, G., Yang, W., Lin, Z., Zhang, X., et al. (2020). Phenomics-based GWAS analysis reveals the genetic architecture for drought resistance in cotton. Plant Biotechnol. J. **18**:2533–2544.

Li, J., Li, Y., Yin, Z., Jiang, J., Zhang, M., Guo, X., Ye, Z., Zhao, Y., Xiong, H., Zhang, Z., et al. (2017). Os ASR 5 enhances drought tolerance through a stomatal closure pathway associated with ABA and H_2O_2 signalling in rice. Plant Biotechnol. J. **15**:183–196.

Liu, H., Mei, H., Yu, X., Zou, G., Liu, G., and Luo, L. (2006). Towards improving the drought tolerance of rice in China. Plant Genet. Resour. **4**:47–53.

Lou, Q., Chen, L., Mei, H., Wei, H., Feng, F., Wang, P., Xia, H., Li, T., and Luo, L. (2015). Quantitative trait locus mapping of deep rooting by linkage and association analysis in rice. J. Exp. Bot. **66**:4749–4757.

Luo, L. (2010). Breeding for water-saving and drought-resistance rice (WDR) in China. J. Exp. Bot. **61**:3509–3517.

Luo, L., and Zhang, Q. (2001). The status and strategy on drought resistance of rice (Oryza sativa L.). Chin. J. Rice Sci. **15**:209.

Margarido, G.R.A., Souza, A.P., and Garcia, A.A.F. (2007). OneMap: software for genetic mapping in outcrossing species. Hereditas **144**:78–79.

Moon, S.J., Kim, H.Y., Hwang, H., Kim, J.A., Lee, Y., Min, M.K., Yoon, I.S., Kwon, T.R., and Kim, B.G. (2017). A dominant negative OsKAT2 mutant delays light-induced stomatal opening and improves drought tolerance without yield penalty in rice. Front. Plant Sci. **8**:772.

Nguyen, V.N., Lee, S.B., Suh, M.C., An, G., and Jung, K.H. (2018). OsABCG9 is an important ABC transporter of cuticular wax deposition in rice. Front. Plant Sci. **9**:1–11.

Oladosu, Y., Rafii, M.Y., Samuel, C., Fatai, A., Magaji, U., Kareem, I., Kamarudin, Z.S., Muhammad, I., and Kolapo, K. (2019). Drought Resistance in Rice from Conventional to Molecular Breeding: A Review. Int. J. Mol. Sci. **20**:3519.

Park, G.G., Park, J.J., Yoon, J., Yu, S.N., and An, G. (2010). A RING finger E3 ligase gene, Oryza sativa Delayed Seed Germination 1 (OsDSG1), controls seed germination and stress responses in rice. Plant Mol. Biol. **74**:467–478.

Peñuelas, J., Piñol, J., Ogaya, R., and Filella, I. (1997). International Journal of Remote Estimation of plant water concentration by the reflectance Water Index WI (R900/R970). Int. J. Remote **18**:2869–2875.

Pollmann, O., Behnassi, M., and Gupta, H. (2019). Climate Change, Food Security and Natural Resource Management: Regional Case Studies from Three Continents (Springer).

Price, A.H., Young, E.M., and Tomos, A.D. (1997). Quantitative trait loci associated with stomatal conductance, leaf rolling and heading date mapped in upland rice (*Oryza sativa*). New Phytol. **137**:83–91.

Ren, R., Li, D., Zhen, C., Chen, D., and Chen, X. (2019). Specific roles of Os4BGlu10, Os6BGlu24, and Os9BGlu33 in seed germination, root elongation, and drought tolerance in rice. Planta **249**:1851–1861.

Seo, J., Joo, J., Kim, M., Kim, Y., Nahm, B.H., Song, S.I., Cheong, J., Lee, J.S., Kim, J., and Choi, Y.D. (2011). OsbHLH148 , a basic helix-loop-helix protein , interacts with OsJAZ proteins in a jasmonate signaling pathway leading to drought tolerance in rice. Plant J. **65**:907–921.

Song, J.-M., Xie, W.-Z., Wang, S., Guo, Y.-X., Koo, D.-H., Kudrna, D., Gong, C., Huang, Y., Feng, J.-W., Zhang, W., et al. (2021a). Two gap-free reference genomes and a global view of the centromere architecture in rice. Mol. Plant **14**:1757–1767.

Shao, Y., Zhou, H.Z., Wu, Y., Zhang, H., Lin, J., Jiang, X., He, Q., Zhu, J., Li, Y., Yu, H., and Mao, C. (2019). OsSPL3, an SBP-domain protein, regulates crown root development in rice. The Plant Cell **31**:1257–1275.

Song, P., Wang, J., Guo, X., Yang, W., and Zhao, C. (2021b). High-throughput phenotyping: Breaking through the bottleneck in future crop breeding. Crop J. **9**:633–645.

Sreenivasulu, N., Jr, V.M.B., Misra, G., Cuevas, R.P., Anacleto, R., and Kishor, P.B.K. (2015). Designing Climate-Resilient Rice with Ideal Grain Quality Suited for High-Temperature Stress, 66, pp. 1737–1748.

Tang, Z., Chen, Z., Gao, Y., Xue, R., Geng, Z., Bu, Q., Wang, Y., Chen, X., Jiang, Y., Chen, F., et al. (2023). A Strategy for the Acquisition and Analysis of Image-Based Phenome in Rice during the Whole Growth Period. Plant Phenomics **5**:0058.

Uga, Y., Sugimoto, K., Ogawa, S., Rane, J., Ishitani, M., Hara, N., Kitomi, Y., Inukai, Y., Ono, K., Kanno, N., et al. (2013). Control of root system architecture by DEEPER ROOTING 1 increases rice yield under drought conditions. Nat. Genet. **45**:1097–1102.

Uga, Y., Kitomi, Y., Ishikawa, S., and Yano, M. (2015). Genetic improvement for root growth angle to enhance crop production. Breed Sci. **65**:111–119.

Wang, Y., Jiang, C., Zhang, X., Yan, H., Yin, Z., Sun, X., Gao, F., Zhao, Y., Liu, W., Han, S., et al. (2024). Upland rice genomic signatures of adaptation to drought resistance and navigation to molecular design breeding. Plant Biotechnol. J. **22**:662–677.

Wu, J., Feng, F., Lian, X., Teng, X., Wei, H., Yu, H., Xie, W., Yan, M., Fan, P., Li, Y., et al. (2015). Genome-wide Association Study (GWAS) of mesocotyl elongation based on re-sequencing approach in rice. BMC Plant Biol. **15**:218.

Wu, X., Feng, H., Wu, D., Yan, S., Zhang, P., Wang, W., Zhang, J., Ye, J., Dai, G., Fan, Y., et al. (2021). Using high-throughput multiple optical phenotyping to decipher the genetic architecture of maize drought tolerance. Genome Biol. **22**:185.

Xia, H., Zhang, X., Liu, Y., Bi, J., Ma, X., Zhang, A., Liu, H., Chen, L., Zhou, S., Gao, H., et al. (2022). Blue revolution for food security under carbon neutrality: A case from the water-saving and drought-resistance rice. Mol. Plant **15**:1401–1404.

Xiong, H., Yu, J., Miao, J., Li, J., Zhang, H., Wang, X., Liu, P., Zhao, Y., Jiang, C., Yin, Z., et al. (2018). Natural variation in *OsLG3* increases drought tolerance in rice by inducing ROS scavenging. Plant Physiol. **178**:451–467.

Xu, K., Lou, Q., Wang, D., Li, T., Chen, S., Li, T., Luo, L., and Chen, L. (2023). Overexpression of a novel small auxin-up RNA gene, OsSAUR11, enhances rice deep rootedness. BMC Plant Biol. **23**:319.

Xu, Y., Li, Z.K., and Thomson, M.J. (2012). Molecular breeding in plants: Moving into the mainstream. Mol. Breed. **29**:831–832.

Yan, W.H., Wang, P., Chen, H.X., Zhou, H.J., Li, Q.P., Wang, C.R., Ding, Z.H., Zhang, Y.S., Yu, S.B., Xing, Y.Z., et al. (2011). A major QTL, Ghd8, plays pleiotropic roles in regulating grain productivity, plant height, and heading date in rice. Mol. Plant **4**:319–330.

Yang, K., Mo, J., Luo, S., Peng, Y., Fang, S., Wu, X., Zhu, R., Li, Y., Yuan, N., Zhou, C., et al. (2023). Estimation of Rice Aboveground Biomass by UAV Imagery with Photosynthetic Accumulation Models. Plant Phenomics **5**:56.

Yang, L., Chen, Y., Xu, L., Wang, J., Qi, H., Guo, J., Zhang, L., Shen, J., Wang, H., Zhang, F., et al. (2022a). The OsFTIP6-OsHB22-OsMYBR57 module regulates drought response in rice. Mol. Plant **15**:1227–1242.

Yang, M.K., Yang, Y.H., Chen, Z., Zhang, J., Lin, Y., Wang, Y., Xiong, Q., Li, T., Ge, F., Bryant, D.A., et al. (2014). Proteogenomic analysis and global discovery of posttranslational modifications in prokaryotes. Proc. Natl. Acad. Sci. USA **111**:E5633–E5642.

Yang, W., Feng, H., Zhang, X., Zhang, J., Doonan, J.H., Batchelor, W.D., Xiong, L., and Yan, J. (2020). Crop Phenomics and High-Throughput Phenotyping: Past Decades, Current Challenges, and Future Perspectives. Mol. Plant **13**:187–214.

Yang, X., Liu, C., Niu, X., Wang, L., Li, L., Yuan, Q., and Pei, X. (2022b). Research on lncRNA related to drought resistance of Shanlan upland rice. BMC Genom. **336**.

Yoshimoto, M., Oue, H., and Kobayashi, K. (2005). Energy balance and water use efficiency of rice canopies under free-air CO_2 enrichment. Agric. For. Meteorol. **133**:226–246.

You, J., Zong, W., Li, X., Ning, J., Hu, H., Li, X., Xiao, J., and Xiong, L. (2013). The SNAC1-targeted gene OsSRO1c modulates stomatal closure and oxidative stress tolerance by regulating hydrogen peroxide in rice. J. Exp. Bot. **64**:569–583.

Yu, D., Ranathunge, K., Huang, H., Pei, Z., Franke, R., and Schreiber, L. (2008). Wax Crystal-Sparse Leaf1 encodes a – ketoacyl CoA synthase involved in biosynthesis of cuticular waxes on rice leaf. Planta **228**:675–685.

Yu, Z., Chen, Y., Zhou, Y., Zhang, Y., Li, M., Ouyang, Y., Chebotarov, D., Mauleon, R., Zhao, H., Xie, W., et al. (2023). Rice Gene Index: a comprehensive pan-genome database for comparative and functional genomics of Asian rice. Molecular plant **16**:798–801.

Yu, S., Huang, A., Li, J., Gao, L., Feng, Y., Pemberton, E., and Chen, C. (2018). OsNAC45 plays complex roles by mediating POD activity and the expression of development-related genes under various abiotic stresses in rice root. Plant Growth Regul. **84**:519–531.

Yue, B., Xue, W., Xiong, L., Yu, X., Luo, L., Cui, K., Jin, D., Xing, Y., and Zhang, Q. (2006). Genetic basis of drought resistance at reproductive stage in rice: Separation of drought tolerance from drought avoidance. Genetics **172**:1213–1228.

Zhou, W.Q., Zhou, Y.Q., He, C.Y., Mou, B.Q., and Zhou, W. (2020). Over-Expression of Oshox4 Enhances Drought and Salinity Tolerance in Rice. Russ. J. Plant Physiol. **67**:1152–1162.